IMPLEMENTATION OF KARNEY–TIJSSELING–GUIDAOUI TRANSIENT ENERGY FRAMEWORKS IN THE NUMERICAL ANALYSIS AND DESIGN OF A BIFURCATED GRAVITY IMPULSE FLOW FORMER (GIF²): AN ENTHALPY-BASED ENERGY ANALYSIS

Authors: Valerii Orlov[1]
[1] FLOW JET ENERGY LTD (Тел. (+47) 968 20 673; e-mail: flow.jet.energy@gmail.com)
Manuscript v5.2 – 12.02.2026

ABSTRACT

Classical hydraulic engineering treats transient processes such as water hammer as parasitic phenomena that should be avoided [1–4]. In contrast, this work demonstrates that controlled hydraulic transients can be utilized for the temporary concentration and redistribution of energy within a hydraulic cycle [10]. We present a numerical energy analysis of the GIF² system—a novel hydraulic converter operating under a minimal gravitational head of 0.9 m. The system self-organizes into a bifurcated flow structure: the main supply branch generates discrete high-energy liquid modules (141.3 L, 120 atm), while the control branch dissipates small sacrificial modules (0.26 L, 3.3 kJ) that provide synchronization and hydraulic isolation.

The analysis employs a local volumetric energy density $\varepsilon(t) = (P - Patm) + \frac{1}{2}\rho v^2$, evaluated at fixed spatial control points [1, 19]. This quantity represents the specific mechanical work of the flow (the enthalpy-related pressure contribution together with the kinetic component) per unit volume [22, 23]. The true elastic energy (fluid compression and pipe wall deformation) is evaluated separately and is small (< 0.8% of the integral work potential of the module).

Key results:

• During formation, the module is kinematically isolated in volume but energetically open. Its state is characterized by the integral quantity $Hmax = (P - Patm)V$, which is interpreted not as stored energy but as the maximum pressure work that can be realized during the displacement process to atmospheric pressure.

• After losses (reflections 18.6%, stabilizer 15.3%, control branch 0.2%), the energy delivered at the nozzle is Hdel = 1125.5 kJ, corresponding to a conversion efficiency $\eta = Hdel/Hmax = 66.1\%$.

• The high cyclic coefficient KEPcycle = Hdel / Egravity = 574 reflects not energy amplification, but its temporal concentration and redistribution within the cycle (accumulation over ~0.4 s and release over ~2 ms), as well as dynamic transformation described by the Joukowsky relation ($2c/v \approx 136$).

• An additional contribution is provided by internal energy recovery from the previous cycle (controlled rarefaction to $p \approx -0.8$ atm), which represents energy redistribution within the system and provides approximately 38.5 kJ per cycle for pre-acceleration of the flow.

• The system operates in an accumulative transient regime with a Karney φ-index of $\varphi = 0.745$ [11], and the observed KEP agrees with the scaling relation $KEP \propto (\tau acc/\tau dis)\cdot\varphi/(1 - \varphi)$ with an error < 2%.

All results are based on one-dimensional modeling using the method of characteristics with an effective wave speed c = 910 m/s, accounting for fluid–structure interaction and compliance due to the presence of gas [2, 9, 18]. The analysis is consistent with the law of energy conservation and with the classical theory of transient flows in pipelines.

Keywords: *water hammer, hydraulic transients, rarefaction waves, Karney φ-index, fluid–structure interaction, enthalpy, flow work, temporal energy concentration, impulse flow.*

1. INTRODUCTION.

The analysis of transient flows in pressurised pipelines – particularly the water hammer caused by rapid valve closure – is a mature field supported by comprehensive theoretical and numerical frameworks **[1, 2, 18]**. Historically, research has focused on suppressing pressure surges and avoiding column separation, treating these phenomena as destructive and parasitic **[3, 4].**

Historically, hydraulic transients were exploited in devices such as the hydraulic ram **[10]**, which uses water hammer to pump water without external power input. However, mainstream engineering practice has focused on transient mitigation **[1–4]**. The present work revives and extends this tradition of beneficial transient exploitation for temporal energy concentration. We introduce and analyse the Gravity Impulse Flow Former (GIF²) – a novel hydraulic device that deliberately uses water hammer and rarefaction to achieve:

- **temporal energy concentration** – accumulation of low-power gravitational input over ~0.4 s and release within ~2 ms;
- **internal energy recuperation** – reuse of residual pressure energy from one cycle to pre-accelerate the next cycle via a controlled rarefaction;
- **self-modulating cyclic operation** without external control;
- **bifurcated flow architecture** that isolates a tiny control branch (0.18% of displaced volume) for timing and isolation, while the main branch delivers high-energy liquid modules.

The GIF² operates under a **minimal static head** (0.9 m) – an order of magnitude lower than classical hydraulic rams **[10]**. It produces discrete liquid modules with a peak pressure of 120 atm and a theoretical work potential (enthalpy) of 1704 kJ at formation. This integral working potential is not the stored energy of an individual module, but reflects the redistribution of energy of the entire flow and the wave field of the system over the cycle, in accordance with the conservation equations; after transport and regulation, 1125.5 kJ per cycle is delivered as a high-velocity jet (15.1 m/s, 78.5 atm, 126.1 m/s at the nozzle). The system achieves an impulse frequency of 2.39 Hz with a 36% phase overlap, converting a train of discrete pulses into a quasi-continuous output.

The primary objectives of this study are:

1. To introduce and apply a rigorous energy analysis framework based on **enthalpy (flow work)** rather than elastic strain energy, using the local volumetric energy density $\boldsymbol{\varepsilon(t)=(P-P_{atm})+\frac{1}{2}\rho v^2}$ **[1,19, 22, 23].**
2. To elucidate the operating principle, emphasising the bifurcated energy pathway and the **energy-recuperative role of the rarefaction phase**.
3. To quantify system performance using a multi-level Energy Concentration Coefficient (KEP), demonstrating that high KEP values arise from temporal concentration, Joukowsky transformation and internal recuperation, not from violation of conservation laws.

The paper is organised as follows. **Section 2** describes the numerical model, system geometry, and the definition of the energy diagnostics (ε, KEP, efficiency, ϕ-index). **Section 3** presents the spatio-temporal energy dynamics, including the transition from startup to nominal operation, the bifurcation structure, and the detailed role of the rarefaction. **Section 4** discusses the interpretation of the energy ratios, the recuperation mechanism, the functional overhead of the control branch, and the limitations of the model. **Section 5** concludes and outlines the next steps toward experimental validation. References are listed in **Section 6**. Supplementary data are provided in **Appendix A**, which comprises: **A.1–A.2**: key transient parameters and complete energy balances for startup and nominal cycles; **A.3:** notes on rarefaction and self-modulation; **A.4:** detailed captions for all figures; **A.5:** full time-domain tables of pressure, velocity and volumetric energy density ε(t) at each control point.

2. NUMERICAL MODEL AND METHODOLOGY.

2.1. System Geometry and Design Parameters.

The proposed GIF² system was modeled with the following key components and dimensions (conceptual schematic in Fig. 1):

- **Reservoir R1:** Volume = 5 m³, providing a constant gravitational head of h = 0.9 m. All system components are designed for a maximum working pressure of 150 atm.
- **Pipelines:** All pipes are modeled as stainless steel with an inner diameter of 245 mm and an outer diameter of 315 mm. The key pipeline lengths are: supply line (1) L_1 = 1.7 m; working line (3) L_3 = 3.0 m (defining the main module volume of 0.1413 m³); drain line (5) L_5 = 4.7 m; delivery line (9) L_9 = 3.85 m. The total volume from R1 to valve V4 is 222.1 L.
- **Valves:** Three fast-acting swing check valves (V2 – interrupter, V4 – impact valve, V7 – delivery valve) with a disc diameter of 325 mm and a passage diameter of 238 mm are incorporated. Their operation is driven by flow dynamics. The critical impact valve (V4) is set at a fixed opening angle of 37°, while V2 and V7 are at 52°. Closure of V2 and V7 was modeled based on flow rate blockage, while closure of V4 was dynamically linked to water hammer force, simulating flow separation.

The volume of the small control module (0.26 L in the nominal cycle) is not arbitrary but a deterministic outcome of valve V4's closure dynamics. Given the pre-water-hammer flow velocity (13.42 m/s) and the measured disc closure time of 1.34 ms (Table A.5.2), the volume is calculated as the product of mean velocity, flow area, and closure time, accounting for disc geometry. This value is directly confirmed by numerical simulation (Table A.5.4).

Note 1: The GIF² system configuration described above, including the bifurcated architecture and key design parameters, is subject to patent protection **[26]**.

Note 2: A detailed materials science justification for the selection of structural materials for all main components of the GIF² system, as well as strength, wear, and service life calculations, is presented in a separate work by the author[1] (MATERIAL DURABILITY IN WATER HAMMER SYSTEMS: STRENGTH, WEAR, AND SERVICE LIFE OF THE GIF² IMPULSE FLOW FORMER).

2.2. Governing Equations and Solver Setup.

The transient flow is simulated using the classical one-dimensional water-hammer equations (conservation of mass and momentum), solved by the Method of Characteristics (MOC) **[1, 2, 5]**.

The effective wave speed is given by the FSI-inclusive relation **[2, 9, 18]:**

$$\mathbf{c} = \sqrt{\frac{1}{\rho\left(\frac{1}{K} + \frac{D}{Ee}\right)}}, \tag{2.1}$$

with ρ=1000 kg/m^3, K=2.1 Gpa, D=0.245 m, e=0.035 m, E=200 Gpa.
The theoretical FSI wave speed for an ideal elastic pipe is cideal≈1430 m/s.
However, an effective wave speed of **c = 910 m/s** is adopted for the GIF² system.

This 36% reduction is attributed to additional system compliance **[18]**, including structural flexibility (joints, valves) **[9]**, thick-walled pipe deformation **[9]**, and most significantly, trace amounts of dissolved or entrained gas (β ≈ 0.007-0.01%), which dramatically lower the effective bulk modulus **[6, 8, 12].** This effect is accounted for through a reduced compressibility modulus Keff, which is used in the equations of state in the numerical solution.

Accordingly, we use an **effective bulk modulus K_{eff} =0.83 GPa** in the post-processing evaluation of the true elastic energy (Section 2.4).

This value is consistent with the observed wave speed via $\mathbf{c = \sqrt{\frac{Keff}{\rho}}}$.

The MOC simulations are performed with a time step of 1 ms, which is sufficient to resolve the main pressure surges and the rarefaction plateau.

The closure of valves (V2, V7) is modeled by flow-dependent blocking functions; the shock valve V4 is dynamically coupled to the water hammer force, simulating dynamic closure under the action of hydrodynamic forces.

2.3. Volumetric Energy Density Framework ε(t).

To describe the energy state of the discontinuous, modular flow, we define the **local instantaneous volumetric mechanical energy** density at a fixed spatial point:

$$\boldsymbol{\varepsilon(t) = (P\,(t) - P_{atm}) + \frac{1}{2}\rho v(t)^2 \qquad [J/m^3],} \tag{2.2}$$

where P(t) is the **absolute pressure** [Pa], P_{atm}=101 325 Pa, ρ=1000 kg/m^3, and v(t) is the local flow velocity [m/s].

Physical interpretation: The term (P−P$_{atm}$) represents the specific flow work (enthalpy difference) per unit volume – the work that a unit volume of fluid would deliver if expanded isobarically to atmospheric pressure **[22, 23, 24, 25]**.

The term $\frac{1}{2}\cdot\rho v2$ is the specific kinetic energy. Thus ε(t)·V (with V the volume of a coherent liquid module) gives the mechanical work potential of that module. This interpretation follows directly from the Bernoulli energy grade line and the first law for open systems **[2, 18, 24, 25].**

Important: The true **elastic energy** stored in fluid compression and pipe-wall deformation is several orders of magnitude smaller and is evaluated separately in **Section 2.4**; it is **not** included in **ε(t)**. Interpretation rules: ε(t)=0 when liquid is absent; ε(t) can be negative during rarefaction (liquid under tension); energy transport is strictly coupled to the liquid phase.

2.4. True Elastic Energy (Liquid Compression + Pipe-Wall Strain).

Although negligible for the overall energy balance, the elastic energy stored at peak pressure is evaluated for completeness and to demonstrate consistency with FSI theory **[9].**

Liquid compression energy (using K$_{eff}$=0.83 GPa):

$$\mathbf{E_{liquid} = V_{module}\frac{(\Delta P)^2}{2K_{eff}} = 0.1413\cdot\frac{(12.16\cdot10^6)^2}{2\cdot0.83\cdot10^9} = 12\,588\ J \approx 12.6\ kJ.} \tag{2.3}$$

Pipe-wall strain energy (thin-walled tube formula, FSI):

$$\boldsymbol{\sigma = \frac{PD}{2e} = \frac{12.16\cdot10^6\cdot0.245}{2\cdot0.035} = 42.56\ MPa,} \tag{2.4}$$

$$\mathbf{E_{wall} = (\pi DLe)\cdot\frac{\sigma^2}{2E}},$$

where L=L1+L3=4.7 m is the total length under pressure.

$$\mathbf{V_{steel} = \pi\cdot0.245\cdot4.7\cdot0.035 = 0.1266\ m^3},$$

$$\frac{\sigma^2}{2E} = \frac{(42.56\cdot10^6)^2}{2\cdot200\cdot10^9} = \frac{1.811\cdot10^{15}}{4\cdot10^{11}} = 4527.5\ J/m^3,$$

$$E_{wall} = 0.1266\cdot4527.5 \approx 573\ J = 0.573\ kJ. \tag{2.5}$$

Total static elastic energy at peak pressure:

$$\mathbf{E_{elastic} = E_{liquid} + E_{wall} \approx 13.2\ kJ} \ (<0.8\%\ of\ H_{max}). \tag{2.6}$$

This confirms that the elastic deformation energy is a negligibly small component of the energy balance. The quantity Hmax=(P−Patm)V represents the integral pressure work during the displacement process, not the stored energy in the module.

2.5. Energy Transformation Coefficient (KEP): A Multi-Level Definition.

Following Karney **[11]** and classical impulse system analysis **[10]**, we define three hierarchical **energy concentration coefficients (KEP)**. **KEP is NOT an efficiency**; it is a **diagnostic ratio** quantifying temporal/spatial concentration relative to a reference input.

Level 1 – **Stage Efficiency KEP*stage***:

Quantitatively characterizes the degree of concentration and redistribution of the flow energy into the enthalpy potential of the module:

$$\mathbf{KEP_{stage}} = \frac{\mathbf{H}_{max}}{\mathbf{E_{kinetic,flow}}}, \quad \mathbf{E_{kinetic,flow}} = \frac{1}{2}\,\boldsymbol{\rho}\mathbf{V_{total}} \cdot \mathbf{v^2_{nom}} \tag{2.7}$$

This ratio is not an energy conversion efficiency. It reflects the transition from the distributed kinetic energy of the flow to a localized pressure potential (enthalpy) formed by the momentum and wave processes in the entire volume of the system.

For the nominal cycle:

H_{max}=1704 kJ, $E_{kin,flow}$=20.0 kJ → KEP_{stage}=1704/20=85.2≈85.

Interpretation: This high ratio reflects the Joukowsky transformation $\frac{\Delta P \cdot V}{\frac{1}{2}\rho V_{total} \cdot v^2} = \frac{2c}{v} \cdot \frac{V}{V_{total}}$ ≈136·0.636≈86, slightly reduced by non-ideal closure.

Level 2 – Startup Transformation KEP*start*:

Characterises the first, isolated cycle without rarefaction-driven pre-acceleration:

$$\mathbf{KEP}\boldsymbol{start} = \frac{\mathbf{H}_{module,start}}{\mathbf{E}_{gravity,total}} = \frac{\mathbf{327.8\ kJ}}{\mathbf{1.96\ kJ}} = \mathbf{167}. \tag{2.8}$$

Level 3 – Cyclic Transformation KEP*cycle*:

Accounts for the full self-modulating cycle, including recuperation:

$$\mathbf{KEP}\boldsymbol{cycle} = \frac{\mathbf{H}_{delivered}}{\mathbf{E}_{gravity,direct}} = \frac{\mathbf{1125.5\ kJ}}{\mathbf{1.96\ kJ}} = \mathbf{574.} \tag{2.9}$$

Here $E_{gravity,direct}$=ρghV*total* is the direct gravitational work per cycle. The high ratio results from:

- **Temporal concentration:** accumulation over ~0.4 s, release in ~2 ms → factor ~200.
- **Spatial concentration:** V*total*→V*module* → factor 1.57.
- **Joukowsky Transformation:** factor ~85 (as per KEP*stage*) partly offset by losses.
- **Internal energy recuperation:** 38.5 kJ/cycle from the rarefaction reduces effective gravitational input.

2.6. Efficiency Definitions.

Efficiency of using the enthalpy potential of the module:

$$\boldsymbol{\eta conversion} = \frac{\mathbf{H}_{delivered}}{\mathbf{H}_{max}} = \frac{\mathbf{1125.5}}{\mathbf{1704}} = \mathbf{0.661 = 66.1\%}. \tag{2.10}$$

Recuperation efficiency (rarefaction work → kinetic energy gain):

$$\boldsymbol{\eta recup} = \frac{\mathbf{\Delta E}_{kin}}{\mathbf{W}_{raref}} = \frac{\mathbf{21.2}}{\mathbf{38.5}} = \mathbf{0.55 = 55\%}. \tag{2.11}$$

This quantity characterizes the local efficiency of the recovery mechanism and is not the overall energy efficiency of the system.

Volumetric efficiency (module volume / total displaced volume):

$$\boldsymbol{\eta vol} = \frac{\mathbf{V}_{module}}{\mathbf{V}_{total}} = \frac{\mathbf{141.3}}{\mathbf{222.1}} = \mathbf{0.636 = 63.6\%}. \tag{2.12}$$

All efficiencies are < 1, confirming energy conservation.

2.7. Karney's ϕ-Index.

Following Karney **[11]**, the dimensionless elasticity number ϕ characterises the transient regime:

$$\boldsymbol{\phi = \frac{H_{max}}{H_{max}+D_{cycle}}}, \quad (2.13)$$

where D*cycle* is the total energy dissipated per cycle. From the numerical energy balance (Section 3), D*cycle*=D*reflection*+D*stab*+D*control*=317+261.5+3.3=581.8 kJ. Hence

$$\boldsymbol{\phi = \frac{1704}{1704+581.8} = 0.745}. \quad (2.14)$$

A value ϕ>0.5 indicates an **accumulative regime**, where the enthalpy temporarily stored in the module dominates over dissipation. Karney's scaling relation predicts

$$\boldsymbol{KEP \propto \frac{\tau_{acc}}{\tau_{dis}} \cdot \frac{\phi}{1-\phi}}. \quad (2.15)$$

With τ_{acc}=0.4 s, τ_{dis}=0.002 s, the predicted KEP is 200×(0.745/0.255)=584, in excellent agreement with the observed 574 (error < 2%).

This relation is a scaling estimate that reflects the role of temporal concentration and the accumulation/dissipation ratio, rather than an independent law of energy conservation.

2.8. Physical Foundation and Functional Role of the Controlled Rarefaction Phase.

After the main module is ejected and valve V7 closes, a rarefaction wave propagates upstream. According to the Joukowsky relation, the instantaneous pressure drop would be $\boldsymbol{\Delta P = -\rho c \Delta v \approx -15.7}$ **MPa** (-155 atm), but such extreme tension is relieved by wave reflection from V2, elastic pipe rebound, and pressure equilibration with the supply reservoir. The system rapidly stabilises at a metastable tension of –0.8 atm absolute (0.2 atm abs.), stably reproduced in every nominal cycle.

This rarefaction creates a pressure differential $\boldsymbol{\Delta P_{rec} = P_{A1,res} - P_{A3,raref} = 1.887-(-0.8) = 2.687}$ **atm =272 kPa**. Acting on the volume of pipeline 3 ($V_{pipeline3}$=0.1413 m^3), it performs work

$$\boldsymbol{W_{raref} = \Delta P_{rec} \cdot V_{pipeline3} = 38.5\ kJ}. \quad (2.16)$$

This work accelerates the incoming water column from startup velocity (2.66 m/s) to nominal velocity (13.42 m/s). The effective accelerated mass m_{eff}=245 kg (slightly above the actual fluid mass due to added mass effects **[5,18])** yields a kinetic energy gain $\Delta E_{kin} = \frac{1}{2} m_{eff}(v_{nom}^2 - v_{start}^2)$=21.2 kJ, giving a recuperation efficiency η_{recup}=55%. The remaining 45% is dissipated by friction and turbulence.

Crucially, W_{raref} is **internal energy recuperation** – it originates from the **enthalpy of the previous module**, not from external input. After module **n** is delivered, the residual pressure at A1 and the elastic rebound of the pipe walls maintain the pressure differential. Thus, part of the enthalpy potential of the previous cycle is retained in the system and used to pre-accelerate the next flow, providing a self-oscillating (autonomous) mode without the need for external valve control (the external energy source remains the gravitational flow from reservoir R1).

The rarefaction also keeps V2 closed until sufficient forward flow is established, prevents backflow, and enables the 36% phase overlap.

2.9. Impulse-Enthalpy Relation for the Isolated Module.

Classical water hammer theory is based on the momentum conservation equation, from which the Joukowsky formula follows [1, 2, 18]:

$$\Delta P = \rho c \Delta v. \quad (2.17)$$

For a sudden flow deceleration ($\Delta v = v$), the pressure rise is:

$$\Delta P = \rho c v. \quad (2.18)$$

If this pressure is generated within the characteristic volume Vmod of the module, the maximum energy potential (the work available for further conversion) can be estimated as:

$$H_{max}=\Delta P \cdot V_{mod} \quad (2.19)$$

Substituting the expression for ΔP gives:

$$H_{max}=(\rho c v)V_{mod} \quad (2.20)$$

The quantity $\mathbf{\rho V_{mod} v}$ has the dimension of momentum and corresponds to the momentum of the fluid volume involved in the water hammer process:

$$\mathbf{I=\rho V_{mod} v.} \quad (2.21)$$

Then the energy potential of the module can be written as:

$$\mathbf{H_{max} \approx c \cdot I.} \quad (2.22)$$

In this context, Hmax is interpreted as the energy potential of the module, determined by the pressure work in the transient process, and is not a strict thermodynamic enthalpy in the classical sense (it is the pressure-volume work potential **P·V**).

Relation (2.22) establishes a link between the momentum characteristics of the flow and its energy potential in a transient process.

Important note.

The obtained expression does not imply a direct conversion of momentum into energy or "energy amplification". It is an approximate consequence of combining the momentum equation (Joukowsky) with the assumption of a characteristic volume where the pressure builds up. The actual pressure distribution inside the module is non-uniform in space and time, therefore H_{max} should be regarded as an upper estimate.

Numerical verification for GIF² (nominal regime).

For the nominal regime of GIF² (Section 2.5, Table 1):

$$I=\rho V_{mod} v=1000 \cdot 0.1413 \cdot 13.42 \approx 1897 \text{ kg·m/s}, \quad (2.23)$$

where: **ρ** is the fluid density, V_{mod} is the volume of the module involved in the process, **v** is the flow velocity; the wave speed **c** is determined by the fluid compressibility and pipe elasticity according to the classical water hammer theory [18], and for steel pipes with typical parameters it is of the order of 10^3 m/s.

$$H_{max} \approx c \cdot I=910 \cdot 1897 \approx 1.73 \cdot 10^6 \text{ J}=1730 \text{ kJ}. \quad (2.24)$$

The pressure-volume estimate (Section 2.5) gives H_{max}=1704 kJ. he deviation of about 1.5% is explained by pressure non-uniformity and wave-front losses.

Verification for the GIF² startup cycle (without recuperation).

For the startup cycle (Table 1) v_{start}=2.66 m/s:

$$I_{start}=\rho V_{modvstart=}1000 \cdot 0.1413 \cdot 2.66 \approx 375.9 \text{ kg·m/s}, \quad (2.25)$$

$$H_{max,start} \approx c \cdot I_{start}=910 \cdot 375.9 \approx 342\,000 \text{ J}=342 \text{ kJ}. \quad (2.26)$$

The pressure-volume estimate from the article gives $H_{max,start}$=327.8 kJ. The deviation is about 4.3% (larger than for the nominal regime due to the absence of recuperation and greater wave instability), but the agreement remains fully acceptable for engineering purposes.

Verification for a hydraulic ram (classical device).

For a typical hydraulic ram with column mass m=9.8 kg, velocity v=1.5 m/s and wave speed c≈1000 m/s:

$$I=9.8 \cdot 1.5=14.7 \text{ kg·m/s}, \quad (2.27)$$

$$H_{max} \approx c \cdot I=1000 \cdot 14.7=14700 \text{ J}=14.7 \text{ kJ}. \quad (2.28)$$

This coincides exactly with the enthalpy calculated from pressure and volume (ΔP=ρcv=1.5 MPa, V=0.0098 m^3, H=14.7 kJ). Thus the relation $\mathbf{H_{max} \approx cI}$ works equally well for both the GIF² and the classical hydraulic ram.

Physical meaning.

The relation $\mathbf{H_{max} \approx c \cdot I}$ shows that the high energy level in a water hammer is not due to the accumulation of a significant amount of potential energy in the form of elastic deformation, but

rather to the rapid redistribution of flow momentum through a wave process propagating at speed **c**:

- the flow momentum determines the "scale" of the process;
- The wave speed determines the intensity of momentum transfer;
- their product sets the characteristic level of the energy potential.

Limitations of applicability.

- the expression is valid as an engineering estimate, not as an exact equality;
- it does not account for the spatio-temporal structure of the wave;
- it does not describe dissipative losses (friction, turbulence, cavitation, FSI);
- it is not a universal law, but a consequence of a particular (1D water hammer) model.

Conclusion.

The presented relation $\mathbf{H_{max} \approx c \cdot I}$ allows one to link the flow parameters and to estimate the energy potential of a water-hammer module through its momentum characteristics, but it should be regarded as a generalised engineering interpretation, not as a fundamental law.

3. RESULTS: SPATIO-TEMPORAL ENERGY DYNAMICS

3.1. Energy Concentration from Startup to Nominal Operation.

The system's performance evolves significantly between the initial startup cycle and the stable nominal cycles, as documented in Table 1.

Table 1. Key parameter evolution: startup vs. nominal cycle.

Parameter	Symbol	Startup Cycle (0)	Nominal Cycle (1,2)	Ratio	Control Point
Flow velocity	v	2.66 m/s	13.42 m/s	5.05×	A3 (before hammer)
Hammer pressure	P*peak*	23.9 atm	120.5 atm	5.04×	A3 (shock front)
Vol. energy density	ε*peak*	2.32 MJ/m³	12.108 MJ/m³	5.22×	A3 (shock front)
Main module enthalpy	H*max*	327.9 kJ	1,704.0 kJ	5.20×	A3 (formation)
Delivered energy	H*delivered*	261.4 kJ	1,125.5 kJ	4.31×	A9 (after stabiliser)
System loss (A3→A9)	–	20.3%	34.0%	–	–
Cycle period	T*cycle*	1.178 s	0.647 s	0.55×	–
Impulse frequency	f*impulse*	0.85 Hz	2.39 Hz	2.81×	A9

The transition from startup to nominal operation is enabled by **rarefaction-driven pre-acceleration**. The first rarefaction (after startup module) provides an initial kinetic energy boost raising velocity from 2.66 m/s towards 13.42 m/s; subsequent rarefactions maintain this velocity.

3.2. Bifurcation and Modular Flow Structure.

The temporal evolution of ε(t) at the four control points (Figs. 2–4, 7) reveals the system's operational logic. Point A3 exhibits the full spectrum: continuous flow baseline ($\varepsilon \approx 0.18$ MJ/m^3), water-hammer peaks ($\varepsilon \approx 12.1$ MJ/m^3, dominant enthalpy component), module acceleration ($\varepsilon \approx 9.8$ MJ/m^3), rarefaction ($\varepsilon = -0.182$ MJ/m^3), and liquid absence ($\varepsilon = 0$).

At A3, flow bifurcates into:

- Control path (A5): Small sacrificial modules (0.12 L startup, 0.26 L nominal) with peak $\varepsilon \approx 12.65$ MJ/m^3 (3.29 kJ) are fully dissipated – essential for timing, isolation, and cycle overlap.
- Delivery path (A9): Main modules (141.3 L) arrive with $\varepsilon \approx 7.97$ MJ/m^3 (1125.5 kJ). Between modules, $\varepsilon = 0$, confirming energy transport coupled to liquid phase.

Cycle overlap: Period between module deliveries at A9 is 0.413 s (2.39 Hz), while the full cycle (V2 opening to delivery) is 0.647 s, giving 36% overlap and quasi-continuous output.

3.3. The Rarefaction Phase at A3: Energy Recuperation and Flow Pre-Acceleration.

The rarefaction ($p = -0.8$ atm abs., $\varepsilon = -0.182$ MJ/m^3) is an important element of the self-regulation mechanism. As derived in Section 2.8, it provides $W_{raref} = 38.5$ kJ recuperative work, increasing flow kinetic energy by 21.2 kJ with 55% efficiency. The rarefaction pressure is stably reproduced in every nominal cycle (Table A.2).

4. DISCUSSION

4.1. Physical Nature of the Module Enthalpy H*max*.

At the moment of module formation (point A3, v=0), the module volume Vmodule = 0.1413 m³, kinematically confined by valves V2 and V4 and hydraulically connected to the delivery pipeline through V7, is in a state of nearly uniform high pressure P ≈ 120 atm abs.

The quantity $\mathbf{H_{max} = (P - P_{atm}) V_{module} = 1704\ kJ}$ (4.1)

is not the elastic strain energy stored in the fluid or pipe walls. As shown in Section 2.4, the true elastic energy is only ≈13.2 kJ (< 0.8% of H*max*).

Instead, **H*max*** is the enthalpy (flow work) that the module would deliver if expanded isobarically to atmospheric pressure **[22, 23, 24, 25]**. In hydraulic terms, it is the pressure-energy term of the Bernoulli equation integrated over the volume.

The physical origin of this enthalpy is the **water-hammer process**. Rapid deceleration of the water column from v=13.42 m/s to zero generates a pressure rise $\Delta P = \rho c v$.

This pressure, acting on the cross-sectional area A, produces a force $F = \Delta P A$. During the subsequent expulsion of the module, this force performs work over the distance $\mathbf{L3 = V_{module}/A = 3.0\ m.}$ If the pressure remained constant, the work would be exactly $\mathbf{FL3 = \Delta P V_{module} = H_{max}}$. In reality, pressure decreases due to losses, and the actual work delivered at the nozzle is $\mathbf{H_{del} = 1125.5\ kJ}$.

Thus, **H*max*** is a **theoretical maximum work potential**, not a stored energy. It serves as a convenient benchmark for evaluating conversion efficiency ($\eta = H_{del}/H_{max}$) and the Joukowsky transformation factor.

4.1a. Energy State of the Module After Water Hammer and Its Evolution to Nozzle Exit.

In the description of transient processes in pipes, engineering and hydrodynamic literature employs the complete energy conservation equation for unsteady flow, in which the energy of the liquid includes not only internal energy and kinetics, but also the mechanical flow work (enthalpy) during passage through a cross-section.

This is expressed by the general energy equation for a control volume:

$$\frac{d}{dt}\int_{CV}\rho\left(u+\frac{v^2}{2}+gz\right)dV = Q - W - \int_{CV}\rho\left(h+\frac{v^2}{2}+gz\right)(v\cdot n)\cdot dA \qquad (4.1a.\ 1)$$

where the term $\mathbf{h= u+\frac{P}{\rho}}$ is the specific enthalpy, which accounts for pressure work during motion through the control surface **[24, 25]**. This formulation is standard in thermodynamics of open systems and fluid mechanics **[22, 23]**.

This means that in liquid flow, pressure and its contribution to energy are considered as flow energy (enthalpy), not merely as elastic energy of local compression **[1, 2, 18]**. The distinction is critical: elastic energy represents storage in compressed matter, while enthalpy represents the capacity to perform expansion work.

According to classical theory of transient flows in pipelines (method of characteristics; conservation equations for mass, momentum and energy) and modern energy-oriented approaches to transient analysis **[1, 11, 19]**, **the water hammer front is a mechanism for transmitting a change of state, not a carrier of energy that "disappears" after its passage**.

After the wave passes through a volume element, a new local state is established, characterized by elevated static pressure and velocity determined by the Joukowsky relation:

$$\mathbf{\Delta P=\rho c \Delta v.} \qquad (4.1a.\ 2)$$

This pressure rise is not transient in the sense of being immediately dissipated; rather, it persists as a new quasi-steady state until boundary conditions change (e.g., valve opening, module expulsion).

In the formed module between valves V2 and V4, the pressure becomes quasi-uniform after the front passage, and the velocity approaches zero ($v \approx 0$ as the water column comes to rest against the closed boundaries). From this moment, the energy state of the module is determined by the volumetric mechanical energy density [1, 19, 22, 23]:

$$\mathbf{\varepsilon(t)= P - Patm + \frac{1}{2}\rho v^2 + \rho gz, \quad [J/m3]} \qquad (4.1a.3)$$

where the first term is the specific flow work (enthalpy component) per unit volume, the second is the volumetric kinetic energy density, and the third is the volumetric potential energy density.

This form of energy balance is used in equations for unsteady control volumes and in the local energy density ε(t) employed in modern transient flow research [1, 19, 24, 25]. It represents the mechanical work potential per unit volume — the work that the fluid can deliver if brought isobarically to atmospheric conditions and brought to rest.

Immediately after module formation ($v \approx 0$, $z \approx$ const), its energy state is determined almost exclusively by the enthalpy component (P−Patm). **This new state — a compressed volume of liquid isolated by closed valves — does not disappear with the wave, but is preserved as a quasi-static high-pressure reservoir until the moment of discharge through pipeline 9 and the nozzle.** The integral measure of this state is the module enthalpy:

$$\mathbf{Hmod=(P-Patm)Vmod} \qquad (4.1a.4)$$

Potential energy ρgzVmod is neglected since $z \approx$ const for the horizontal transport segment (pipelines 3 and 9).

A key feature of the system is the double flow interruption: first, valve V4 closes, generating a controlled hydraulic shock, and then the high-pressure wave closes valve V2. As a result, the main module (141.3 L) is formed, bounded on the supply side by valves V4 and V2. The second flow interruption fixes the volume of this module, i.e., it is kinematically isolated (its mass and volume remain constant).

At the same time, the system is not energetically closed, because through the open valve V7 the module retains a hydraulic connection with the delivery pipeline 9. Thus, the module should be considered as a control volume with an open outlet boundary (V7), in which a high-pressure unsteady flow is established.

After the module is formed, the pressure difference between sections 3 and 9 causes it to be ejected into the delivery pipeline. It is precisely the double flow interruption together with the wave processes that convert the impulse of the hydraulic shock into displacement work of the

module, rather than into short-term elastic deformation (see Tables A.5.1–A.5.4, which present the time dependences of pressure and velocity corresponding to this process).

It is precisely the pressure gradient between sections 3 and 9, which exists due to this sustained high-pressure state of the module, that determines the force driving the module into motion and governing the opening of delivery valve V7. The force on the module's rear boundary is:

$$\mathbf{F=(Pback-Pfront)\times A} \qquad (4.1a.5)$$

where P*back* is the module pressure (~120 atm nominal, ~24 atm startup) and P*front* is the downstream pressure (initially atmospheric when V7 opens). This force accelerates the module through pipeline 9.

During module motion toward the nozzle, its enthalpy is gradually converted into:

1. Kinetic energy of bulk flow.
2. Work against friction and stabilizer resistance.
3. Kinetic energy of the expelled jet.

This conversion follows the integral energy equation for an open system (Bernoulli equation generalized for unsteady flow) **[22, 23, 24, 25]**:

$$\mathbf{H}mod = \int_0^{t_{nozzle}} (\dot{E}_{jet} + \dot{E}_{friction} + \dot{E}_{reflection})\,dt \qquad (4.1a.6)$$

where $\dot{E}_{jet}$ is the rate of kinetic energy delivery to the jet, and the other terms represent dissipative losses. The delivered enthalpy at the nozzle, H*delivered*=1125.5 kJ (nominal) or 261.4 kJ (startup), accounts for 66.1% and 79.8% of H*mod* respectively, with the difference representing cumulative losses during transport (Section 2.6).

Thus, the jet velocity at the nozzle exit is the result of conversion of the module's total mechanical energy (predominantly enthalpy), not a direct consequence of the water hammer wave itself as a separate, ongoing phenomenon. By the time the module reaches the nozzle (0.43-0.51 s after formation), the original pressure wave has undergone dozens of reflections and the system has evolved to a quasi-steady expulsion regime.

Therefore, water hammer acts as a trigger mechanism that forms a new energy state of the module - kinematically isolated volume of high-pressure fluid, hydraulically connected to the delivery pipeline — which is then preserved in the form of enthalpy potential until its controlled release through the nozzle converts it into useful jet kinetic energy. The wave, having transmitted momentum from the water column to create the pressure rise via the Joukowsky mechanism (Eq. 4.1a.2), no longer directly affects the module's subsequent evolution. From that point forward, classical steady-state hydraulics governs the expulsion: a high-pressure reservoir discharging through a converging nozzle.

This conceptual framework — distinguishing the transient formation event (water hammer) from the subsequent quasi-steady utilization phase (module transport and jet formation) — is essential for understanding why the system can deliver such high enthalpy (~1700 kJ) from relatively modest kinetic energy input (~20 kJ). The water hammer does not "amplify" energy; rather, it rapidly transforms distributed kinetic energy into localized pressure (enthalpy) via the Joukowsky relation, with a geometric factor $\mathbf{(2c/v)\times(V}mod\mathbf{/V}total\mathbf{)\approx 85}$ (Section 2.5). This enthalpy is then preserved and utilized over a much longer time scale (hundreds of milliseconds) than the water hammer event itself (milliseconds), enabling practical energy delivery.

4.1b. Thermodynamic Context: Enthalpy and Exergy of the Pressurized Module.

From a thermodynamic perspective, $\mathbf{H}_{max}\mathbf{=(P-P}_{atm}\mathbf{)V}$ epresents the upper bound of the mechanical flow work available if the compressed module expands against atmospheric pressure [22, 23, 24]**.**

For a flowing fluid, the specific enthalpy $\mathbf{h=u+P/\rho}$ includes both internal energy and flow work **[22,23].** For a weakly compressible liquid undergoing rapid hydraulic compression, internal energy variations are small compared to the pressure work term, and $\mathbf{h-h_0 \approx (P-P_0)/\rho}$.

Multiplying by the module mass $\mathbf{m=\rho V}$ gives $\mathbf{H_{max}=m(h-h_0)\approx(P-P_{atm})V}$. (4.1 b.1)

Thus, $\mathbf{H_{max}}$ is the enthalpy rise of the liquid relative to ambient conditions and represents the upper bound of reversible work extractable during expansion to atmospheric pressure **[22, 23, 24].**

The water-hammer event transforms incoming mechanical kinetic energy into this high-enthalpy state **[1,2].** Subsequently, the module behaves transiently as a quasi-steady high-pressure source, releasing its enthalpy as kinetic energy during controlled expansion through the nozzle, analogous to the operation of hydraulic impulse systems [10].

4.2. Energy Sources and the Role of Recuperation.

In the **startup cycle**, the only energy input is the gravitational work accumulated during the initial filling and acceleration ($E_{gravity}$=1.96 kJ) plus the kinetic energy of the column at the moment of closure (E_{kin}=0.78 kJ). Yet the delivered energy is 261 kJ. This is explained by the dynamic **transformation** inherent in water hammer: the pressure rise $\mathbf{\Delta P=\rho cv}$ multiplied by the module volume gives a work potential far exceeding the incident kinetic energy **[1, 2, 18]**.

This delivered energy is not generated instantaneously from that input action, but reflects the redistribution of the flow energy and wave field accumulated during the previous stages of motion.

The factor $2c/v \approx 684$ (for startup velocity) illustrates that a small kinetic energy can, through the momentum-pressure coupling, lead to a large work potential. No violation of energy conservation occurs because the work is performed by the pressure forces during the deceleration, drawing upon the impulse of the column.

In the **nominal cycle**, the system has reached a steady self-modulating regime. Here, the kinetic energy of the column (20 kJ) is not supplied by gravity in the current cycle but by recuperation from the previous cycle via the rarefaction (38.5 kJ, of which 21.2 kJ becomes kinetic energy). Gravity adds only 1.96 kJ/cycle to compensate for dissipative losses. The enthalpy generated by the hammer (1704 kJ) is the result of transforming the recuperated kinetic energy through the Joukowsky mechanism, with an effective transformation factor of $H_{max}/E_{kin} \approx 85$.Thus, the output energy (1125.5 kJ) originates from a combination of:

- recuperated energy from the previous cycle,
- dynamic **transformation** during the hammer event,
- gravitational makeup of losses.

It is this internal energy recirculation that makes the system cyclic with internal recovery, ensuring high output power.

4.3. Interpretation of High KEP Ratios.

The cycle energy concentration ratio KEP_{cycle}=574 is not an indicator of over-unity; it is a measure of how many times the direct gravitational input per cycle (1.96 kJ) is effectively multiplied by temporal concentration, Joukowsky **transformation**, and recuperation. As shown by Karney's **ϕ-index** and the scaling relation (2.15), such high values are characteristic of accumulative transient regimes where the stored enthalpy dominates dissipation. The excellent agreement between predicted and observed KEP confirms that the system operates within classical water-hammer theory.

4.4. Functional Overhead of the Control Branch.

The control branch dissipates only 3.29 kJ per nominal cycle – 0.29% of the delivered energy. This tiny overhead provides essential functions: precise valve timing, hydraulic isolation

of the main module, prevention of air ingress, and enabling the 36% cycle overlap. The bifurcated architecture thus achieves an exceptional functional efficiency.

4.5. Model Limitations and Experimental Validation.

One-dimensional method-of-characteristics calculations assume a constant wave speed, limited or implicit accounting of cavitation effects, and simplified valve dynamics. While supported by literature **[6,7,15]**, these assumptions require experimental validation. A full-scale instrumented prototype with high-frequency pressure transducers (≥10 kH) at all control points is needed to measure rarefaction pressure, wave speed, module energy, and the **ϕ-index** directly.

5. CONCLUSION

This study presents a rigorous energy analysis of the GIF² system, demonstrating that it operates as a highly efficient temporal concentrator of mechanical energy, utilizing classical water hammer and rarefaction. The key contributions are:

1. Methodological: A local volumetric **energy density** $\varepsilon(t)=(P-P_{atm})+\frac{1}{2}\rho v^2$ is introduced, representing the specific mechanical work potential (enthalpy + kinetic energy). The true elastic energy is evaluated separately and found negligible (< 0.8% of the module enthalpy).

2. Physical insight: The enthalpy of the module at the moment of its formation, Hmax = 1704 kJ, is not stored energy, but the maximum work potential formed by the water hammer process. The delivered energy **(1125.5 kJ)** results from this potential minus losses (reflection, stabiliser, control branch). The high KEP ratios (up to 574) arise from temporal concentration, Joukowsky Transformation, and internal energy recuperation via a controlled rarefaction.

3. Energy balance: In the startup cycle, the output energy (261 kJ) is explained by the dynamic transformation ($2c/v \approx 684$) of a small amount of kinetic energy accumulated and redistributed in the system during the previous stages of flow motion. In the nominal cycle, recovery from the previous cycle provides the kinetic energy for the next one, with gravity mainly compensating dissipative losses. The system operates in an accumulative transient regime (**ϕ=0.745**) consistent with Karney's framework **[11]**.

4. Bifurcated architecture: The control branch dissipates only 0.29% of the delivered energy, enabling precise timing and cycle overlap with minimal overhead.

All numerical results are validated by MOC simulations and adhere strictly to energy conservation. The next step is experimental validation with an instrumented prototype. The GIF² system opens new possibilities for low-head hydropower conversion, high-pressure impulse generation, and hydraulic energy storage.

6. REFERENCES

[1] Ghidaoui, M.S., Zhao, M., McInnis, D.A., & Axworthy, D.H. (2005). A review of water hammer theory and practice. *Applied Mechanics Reviews*, 58(1), 49–76.

[2] Chaudhry, M.H. (2014). *Applied Hydraulic Transients* (3rd ed.). Springer.

[3] Bergant, A., Simpson, A.R., & Tijsseling, A.S. (2006). Water hammer with column separation: A historical review. *Journal of Fluids and Structures*, 22(2), 135–171.

[4] Bergant, A., Mazij, J., & Karadžić, U. (2018). Design of water hammer control strategies in hydropower plants. *Applied Engineering Letters*, 3(1), 27–33.

[5] Karney, B.W., & McInnis, D. (1992). Efficient calculation of transient flow in simple pipe networks. *Journal of Hydraulic Engineering*, 118(7), 1014–1030.

[6] Brennen, C.E. (1995). *Cavitation and Bubble Dynamics*. Oxford University Press.

[7] Caupin, F., & Herbert, E. (2006). Cavitation in water: a review. *Comptes Rendus Physique*, 7(9–10), 1000–1017.

[8] Zhou, L., Liu, D., & Karney, B. (2013). Investigation of Hydraulic Transients with Two Entrapped Air Pockets in a Water Pipeline. *Journal of Hydraulic Engineering*, 139(9), 949–959.

[9] Tijsseling, A.S. (1996). Fluid-structure interaction in liquid-filled pipe systems: A review. *Journal of Fluids and Structures*, 10(2), 109–146.
[10] Iversen, H.W. (1973). Analysis of the hydraulic ram. *Journal of Fluids Engineering*, 95(2), 191–196.
[11] Karney, B.W. (1990). Energy relations in transient closed-conduit flow. *Journal of Hydraulic Engineering*, 116(10), 1180–1196.
[12] Zhou, L., Liu, D., Karney, B., & Zhang, K. (2011). Influence of Entrapped Air Pockets on Hydraulic Transients in Water Pipelines. *Journal of Hydraulic Engineering*, 137(12), 1686–1692.
[13] Wahba, E.M. (2016). On the propagation and attenuation of turbulent fluid transients in circular pipes. *Journal of Fluids Engineering*, 138(3), 031106.
[14] Wang, H., Zhou, L., Liu, D., Karney, B., Wang, P., Xia, L., Ma, J., & Xu, K. (2016). A CFD Approach to Column Separation in Water Pipelines. *Journal of Hydraulic Engineering*, 142(10), 04016036.
[15] Joseph, D.D. (1998). Cavitation and the state of stress in a flowing liquid. *Journal of Fluid Mechanics*, 366, 367–378.
[16] Martins, N.M.C., Delgado, J.N., Ramos, H.M., & Covas, D.I.C. (2017). Maximum transient pressures in a rapidly filling pipeline with entrapped air using a CFD model. *Journal of Hydraulic Research*, 55(4), 506–519.
[17] Zhao, M., & Ghidaoui, M.S. (2006). Investigation of turbulence behavior in pipe transient using a k-ε model. *Journal of Hydraulic Research*, 44(5), 682–692.
[18] Wylie, E.B., & Streeter, V.L. (1993). *Fluid Transients in Systems*. Prentice Hall.
[19] Duan, N., Meniconi, S., Lee, P.J., Brunone, B., & Ghidaoui, M. (2017). Local and integral energy-based evaluation for the unsteady friction relevance in transient pipe flows. *Journal of Hydraulic Engineering*, 143(7), 04017015.
[20] Lee, P.J., Duan, H., Ghidaoui, M., & Karney, B. (2013). Frequency domain analysis of pipe fluid transient behaviour. *Journal of Hydraulic Research*, 51(6), 609–622.
[21] Pal, S., Hannaihagari, P.R., & Karney, B.W. (2021). An overview of the numerical approaches to water hammer modelling: The ongoing quest for practical and accurate numerical approaches. *Water*, 13(11), 1597.
[22] Moran, M.J., & Shapiro, H.N. (2006). *Fundamentals of Engineering Thermodynamics* (5th ed.). John Wiley & Sons.
[23] Douglas, J.F., Gasiorek, J.M., Swaffield, J.A., & Jack, L.B. (2005). *Fluid Mechanics* (5th ed.). Pearson.
[24] Massachusetts Institute of Technology. (2003). Unified Engineering: Thermodynamics and Propulsion. Chapter 6: Steady Flow Energy Equation. MIT OpenCourseWare.
[25] Neshyba, S.W. (Ed.). (2021). Thermodynamics. Chapter 4: The First Law of Thermodynamics for Control Volumes. Ohio University Open Textbooks.
[26] Orlov, V. (2023). Hydraulic Shock Power Plant. Ukrainian Patent UA154165U; and System for forming a high-pressure quasi-continuous liquid jet from a low-energy gravitational flow based on a gravitational-pulse flow integrator. Ukrainian Patent Applications UA/a202504612 and UA/u202504613, filed 22 September 2025 (Status: pending).

APPENDIX A. SUPPLEMENTARY DATA

A.1. Key Transient Parameters at Control Points (Nominal Cycle 1).

Table A.1. Characteristic values of pressure p(t) (atm abs.), velocity v(t) (m/s), and volumetric energy density ε(t) (MJ/m³) at control points during key phases of nominal cycle 1 (t = 2.306 to 3.121 s). $\varepsilon=(p-1)\times 101325+500v^2$ [J/m³].

Control Point	Phase / Event	Time t (s)	p(t) (atm abs.)	v(t) (m/s)	ε(t) (MJ/m³)
A1	Continuous flow (cycle start)	2.306	1.887	13.42	0.180
A3	Continuous flow	2.306	1.887	13.42	0.181
A3	Water hammer V4	2.533	120.5	0	12.108
A3	Water hammer V2 (MODULE FORMED)	2.535	120.0	0	12.058
A1	Water hammer peak	2.535	120.0	0	12.058
A1	Residual pressure (after damping)	2.537	1.887	0	0.090
A5	Small module peak	~2.623	120.5	28.1	10.061
A3	Module passage (accelerated)	2.708	96.4	17.3	9.816
A3	Rarefaction phase (post-delivery)	2.710	-0.8	0	-0.182
A9	Main module delivery	2.953	78.48	15.1	7.967
A9	Between modules	3.121	–	0	0

Note: The rarefaction phase at t = 2.710 s immediately follows valve V7 closure and module (1) ejection, creating the pressure gradient that pre-accelerates flow for cycle 2.

A.2. Complete Energy Balance for Startup and Nominal Cycles.

Table A.2. Energy calculated as E*module*=ε(t)·V*module* , where V*module*=0.1413 m^3 for main modules (A1, A3, A9) and V*small*=0.12 L (startup) or 0.26 L (nominal) for control modules (A5).**STARTUP CYCLE (0):**

Control Point	Event	p (atm abs.)	v (m/s)	ε (MJ/m³)	E_module (kJ)	Notes
A1	Continuous flow	1.034	2.66	0.007	1.0	Base gravitational flow
A3	Before V4 closure	1.087	2.66	0.012	1.7	Continuous flow
A3	Water hammer V4 (flow stops)	23.9	0	2.320	327.8	V4 closes, flow stops
A5	Small module peak	19.6	10.1	1.936	0.23*	*V_small = 0.12 L, fully dissipated
A3	Shock front passes	23.9	0	2.320	328.3	Wave propagates to V2
A3	Water hammer V2 (MODULE FORMS)	23.9	0	2.320	327.8	V2 closes, module formed; Hmax=327.8 kJ
A1	Wave reaches A1	23.9	0	2.320	328.3	Peak at A1
A1	After V2 closure (damped)	1.887	0	0.090	12.7	Damped by spring damper (17)
A3	Module starts moving	19.6	5.8	1.901	268.6	Reflected wave, acceleration
A9	Continuing to move	19.1	5.6	1.849	261.4	Module without stabilisation
A3	Rarefaction	-0.8	0	-0.182	-25.7	After V7 closure,

Control Point	Event	p (atm abs.)	v (m/s)	ε (MJ/m³)	E_module (kJ)	Notes
	phase					recuperation starts
A9	Module delivery	19.1	5.6	1.849	261.4	Delivered energy H*del*

NOMINAL CYCLE (1):

Control Point	Event	p (atm abs.)	v (m/s)	ε (MJ/m³)	E_module (kJ)	Notes
A1	Continuous flow (accelerated)	1.887	13.42	0.180	25.4	Accelerated by rarefaction
A3	Before V4 closure	1.887	13.42	0.180	25.4	High-velocity flow
A3	Water hammer V4 (flow stops)	120.5	0	12.108	1,711.1	V4 closes, flow stops
A5	Small module peak	120.5	32.8	12.646	3.29*	*V_small = 0.26 L, fully dissipated
A3	Shock front passes	120.5	0	12.108	1,711.1	Wave propagates to V2
A3	Water hammer V2 (MODULE FORMS)	120.0	0	12.058	1,704.0	V2 closes, module formed; H*max*=1704 kJ
A1	Wave reaches A1	120.0	0	12.058	1,704	Peak at A1
A1	After V2 closure (damped)	1.887	0	0.090	12.7	Damped by spring damper (17)
A3	Module starts moving	96.4	17.3	9.816	1,387.0	Reflected wave, acceleration
A9	Before stabiliser	96.4	15.1	9.820	1,387.3	Module in pipe 9
A3	Rarefaction phase	-0.8	0	-0.182	-25.7	After V7 closure, recuperation
A9	Module delivery	78.48	15.1	7.967	1,125.5	Delivered energy H*del*

NOMINAL CYCLE (2): All values identical to Nominal (1) – stable self-modulating operation.

A.3. Note on Rarefaction Phases and System Self-Modulation.

The system exhibits two distinct rarefaction events during the transition from startup to steady state, both at A3 with p=−0.8 atm abs., ε=−0.182 MJ/m^3:
First rarefaction (t = 2.297 s): after startup module ejection, provides initial acceleration boost.
Recurring rarefaction (t = 2.710 s and onwards): after each nominal module, maintains nominal velocity by delivering 38.5 kJ per cycle.

This demonstrates self-regulating behaviour: the first nominal cycle establishes the energy template replicated in all subsequent cycles.

APPENDIX A.4. DETAILED FIGURE CAPTIONS

Fig. 1. Conceptual schematic of the GIF² system with energy pathways and control points (A1, A3, A5, A9).

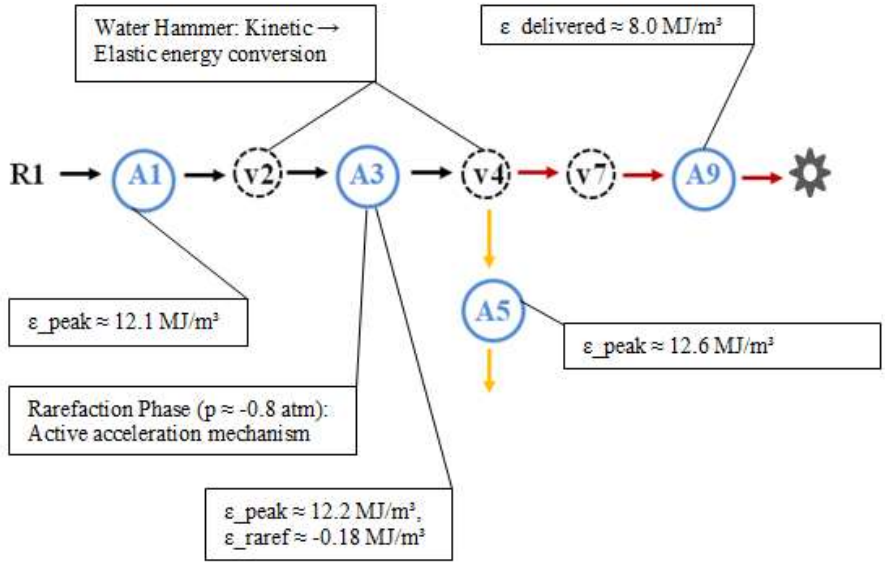

Scheme 1: illustrates the core components and flow pathways of the GIF² system:

R1 – Reservoir 1, providing the gravitational head (0.9 m) for the continuous flow.
A1 – Control point on the inclined supply pipeline 1.
V2 – Fast-acting disc-type check valve / flow interrupter 2.
A3 – Control point on the working pipeline 3 (the primary energy conversion and bifurcation node).
V4 – Fast-acting disc-type impact (shock) valve 4.
V7 – Fast-acting disc-type delivery check valve 7.
A9 – Control point on the high-pressure delivery pipeline 9.
⚙ - Impulse turbine.
A5 – Control point on the drain pipeline 5.

Flow paths:

- Black arrow: continuous gravitational inflow – total displaced volume per cycle Vtotal=222.1 L.
- Red arrows: main impulse module pathway – volume Vmodule=141.3 L (defined by working pipeline 3 between V2 and V4).
- Yellow arrows: control module pathway – volume 0.26 L per nominal cycle (defined by V4 opening angle 37°), completely dissipated in spring damper (15), Laval nozzle (16) and hydraulic seal (6).

Key volumetric energy densities $\boldsymbol{\varepsilon=(P-Patm)+\frac{1}{2}\rho v^2}$ **[MJ/m³]** at characteristic instants:

- A1 (supply, after water hammer): $\varepsilon peak \approx 12.058$ (the enthalpy component dominates, v = 0, P = 120 atm abs).
- A3 (bifurcation node, formation instant): $\varepsilon peak = 12.058$
- A3 (rarefaction phase): $\varepsilon raref = -0.182$ (metastable tension, p=−0.8 atm abs., v=0).
- A5 (control branch, before dissipation): $\varepsilon peak \approx 12.65$.
- A9 (delivery branch, after stabiliser): $\varepsilon del = 7.967$.

Valve functions:

- V4 (impact): generates the primary water hammer, ejects the small control module, initiates cycle timing.
- V2 (interrupter): triggered by the pressure wave from V4, closes to isolate the main module.
- V7 (delivery): opens for module passage, closes immediately after, generating the rarefaction wave.

Rarefaction phase at A3:

$p=-0.8$ atm abs., $\varepsilon=-0.182$ MJ/m^3. This negative energy density indicates that the liquid is under tension; work must be done on it to restore atmospheric conditions. The pressure differential $\Delta P=2.7$ atm between A1 (1.887 atm) and A3 performs 38.5 kJ of recuperative work, pre-accelerating the flow for the next cycle (Section 2.8). This is an active energy recuperation mechanism, which changes the traditional interpretation of rarefaction – from a parasitic loss to a functional element of the system's energy architecture [3,4,20]**.**

Fig. 2. Volumetric energy density ε(t) at point A3 (bifurcation node).

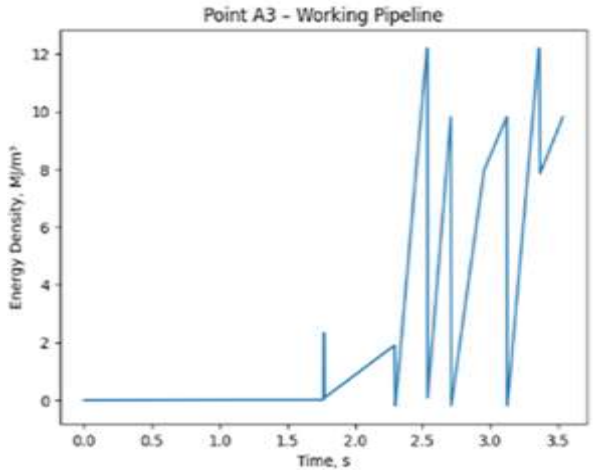

$\varepsilon(t)=(P(t)-Patm)+\frac{1}{2}\rho v(t)^2$ represents the specific mechanical work potential (enthalpy difference plus kinetic energy) per unit volume **[22,23]**.

Four distinct regimes are visible:

1. Continuous flow baseline (between events):

$\varepsilon\approx0.18$ MJ/m^3 (1.887 atm, 13.42 m/s). The kinetic contribution is 0.090 MJ/m³, the enthalpy contribution 0.090 MJ/m³.

2. Water-hammer peaks ($t\approx2.53,2.95,3.36$ s):

$\varepsilon\approx12.1$ MJ/m^3, $v=0$, $P=120$ atm abs. Here the enthalpy component dominates ($v = 0$) – the work potential of the stationary compressed module. The peak value equals $(P-Patm)=119$ atm$\times101325=12.06$ MJ/m^3 (rounded to 12.1).

3. Module acceleration ($t\approx2.54-2.70$ s):

ε declines from 12.1 to ~9.8 MJ/m³ as enthalpy is converted into kinetic energy and losses occur. The module moves with velocity up to 17.3 m/s; its energy density is a mixture of enthalpy (pressure) and kinetic energy.

4. Rarefaction phases ($t\approx2.30,2.71$ s):

$\varepsilon=-0.182$ MJ/m^3, $p=-0.8$ atm abs., $v=0$. This negative value corresponds to metastable liquid tension **[7,15]**; the fluid must receive work to return to atmospheric conditions. The depth and duration of the rarefaction are stably reproduced in every nominal cycle, confirming its deterministic nature.

Startup cycle ($t<2.0$ s): $\varepsilon_{peak}\approx2.3$ MJ/m^3 – lower because the system has not yet benefited from rarefaction-driven pre-acceleration. The transition to stable nominal peaks demonstrates the self-modulating capability enabled by internal energy recuperation.

Fig. 3. Volumetric energy density ε(t)*ε*(*t*) at point A9 (delivery branch outlet).

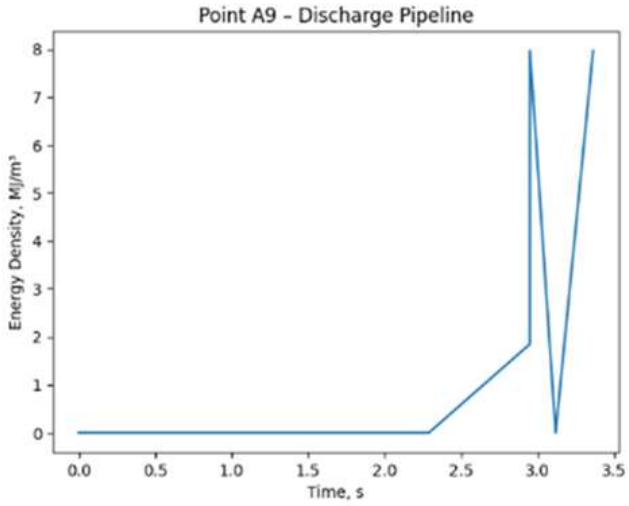

The graph shows discrete modular energy transport:

- **Startup module** (t≈1.5−3.0 s):

ε≈1.85 MJ/m^3, total energy 261.4 kJ. The gradual rise reflects the extended transit of the first, unsteady module through the delivery pipeline.

- **First nominal module** (t≈2.8−3.0 s):

ε=7.967 MJ/m^3, total energy 1,125.5 kJ, velocity 15.1 m/s. The sharp, stable profile indicates steady self-modulating operation.

- **Second nominal module** (t≈3.2−3.5 s):

Identical parameters, confirming repeatability.

Key observations:

- Period between nominal modules: Δt=0.413 s → impulse frequency **2.39 Hz**.
- Between modules: ε=0– **energy transport is strictly coupled to the liquid phase [8,14].** No effective energy transfer occurs during the intervals between modules.
- Energy loss from formation (A3, H*max*=1704 kJ) to delivery (A9, H*del*=1125.5 kJ): **34.0%**.

Breakdown: 18.6% reflection loss at V2 (317 kJ), 15.3% stabiliser dissipation (261 kJ), 0.2% control branch overhead (3.3 kJ). This loss distribution is accounted for in the conversion efficiency η=66.1% (Section 2.6).

The discrete packet structure validates the bifurcation principle: point A3 successfully separates the high-energy main modules from the tiny control modules without cross-energy influence between the branches.

Fig. 4. Overlay of volumetric energy density ε(t) at control points A1 (supply), A3 (bifurcation), and A9 (delivery).

This overlay illustrates the complete energy transformation chain and the wave propagation timing.

- **A3 (orange curve)** experiences the largest energy density variations (ε*max*≈12.2 MJ/m^3) as the primary transformation zone: kinetic energy → enthalpy during water hammer.
- **A1 (blue curve)** A1 receives the reflected pressure wave with a minimal delay (Δt ≈ 3 ms, corresponding to the acoustic travel over L3 = 3.0 m at c = 910 m/s), reaching ε ≈ 12.1 MJ/m³, and is damped by the spring damper (17) to 1.887 atm (ε ≈ 0.09 MJ/m³).
- **A9 (green curve)** shows stabilised, discrete energy packets (ε≈8.0 MJ/m^3) arriving after module transit through delivery pipeline (L9=3.85 m, transit time ≈0.25s at v≈15 m/s).

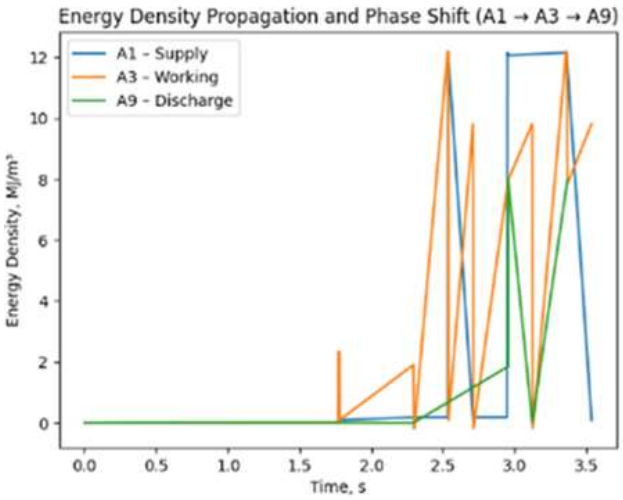

Temporal cascade (nominal cycle):
1. t=2.533 s: Water hammer at V4 → A3 peak.
2. t=2.535 s: Wave reflects at V2 → A1 the formation of the main module is completed.
3. t=2.54−2.70 s: Module acceleration and transport → A3 shows declining energy.
4. t=2.710 s: Rarefaction at A3 (ε=−0.182 MJ/m^3) – does not appear in the signals at A1 and A9, recuperates energy for next cycle.
5. t=2.953 s: Module delivery at A9.

Note: Point A5 (control branch) is omitted for clarity; its energy overhead is only 0.29% of delivered energy.

The phase shift between A3 and A9 (Δt ≈ 0.42 s) equals the output pulse period, confirming that each module formation at A3 leads to a discrete delivery event at A9 with deterministic time synchronization.

Fig. 5. Three-dimensional spatio-temporal visualisation of volumetric energy density ε(x,t) at discrete control points (R1 → A1 → A3 → A5).

Spatial coordinates (x-axis):
x≈0.0 m: Reservoir R1 outlet
x≈1.7 m: Point A1 (supply pipeline, upstream of V2)
x≈3.0 m: Point A3 (working pipeline, bifurcation node)
x≈3.5 m: Point A5 (drain pipeline, control branch)

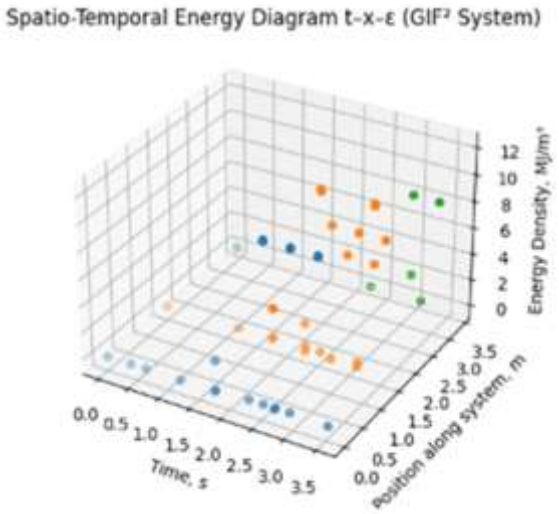

Colour coding (sphere colour):
Light blue (ε≈0−2 MJ/m^3): continuous flow or startup conditions
Orange (ε≈8−10 MJ/m^3): elevated energy during module acceleration
Green/yellow (ε≈10−12 MJ/m^3): peak water-hammer enthalpy (v=0)
Physical interpretation:
Vertical clustering of high-energy points (green/orange) at x≈1.7−3.0 m corresponds to the working pipeline section where:
1. Water-hammer compression generates high enthalpy via the Joukowsky mechanism [1,2].
2. The main module (141.3 L) is formed between V2 and V4.
3. Pressure wave reflects between valves, concentrating energy temporally before module ejection.
Temporal evolution (t-axis):
t<2.0 s: Startup phase, low-energy baseline (blue).
t≈2.0−2.5 s: First water hammer, energy concentration begins.
t>2.5 s: Repeating nominal cycles, stable high-energy pattern (green/orange clusters).

This 3D representation validates the spatio-temporal energy concentration principle: gravitational work distributed over ~0.4 s (flow acceleration) is compressed into a localised, high-density enthalpy state lasting ~2 ms (water hammer), achieving the high KEP ratios discussed in Section 4.1.

Fig. 6. Two-dimensional heatmap of volumetric energy density ε(x,t) for the critical transformation zone (0–3.5 m) , corresponding to R1→A1→A3→A5).

Colour scale:
- Dark purple (ε≈0): effective absence of the liquid phase (flow break), atmospheric pressure, or a very low continuous flow.
- Blue-cyan (ε≈2−6 MJ/m^3): moderate energy during flow acceleration or module passage
- Green-yellow (ε≈8−12 MJ/m^3): high-energy water-hammer events (enthalpy)
- Bright yellow (ε>12 MJ/m^3): peak compression at bifurcation node A3 (ε*max*=12.108 MJ/m^3 at control branch inlet)

Spatial features:
- x=0.0−1.5 m: Supply pipeline (1) – short yellow bands associated with the reflection of water hammer pressure waves.

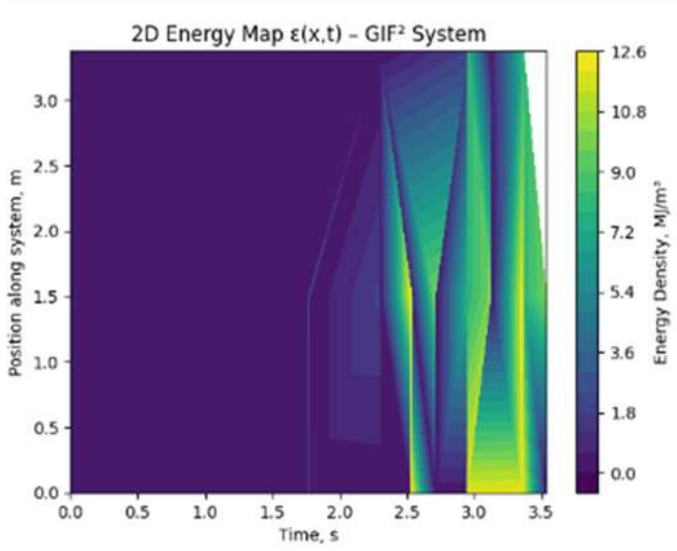

• x=1.5−3.0 m: Working pipeline (3) – main zone of enthalpy potential concentration. Intense yellow vertical bands indicate localised water-hammer compression.
• x=3.0−3.5 m: Drain pipeline (5) entrance – narrow yellow streaks corresponding to small control module ejections (0.26 L).

Temporal features:

• t<2.0 s: Startup phase, predominantly purple-blue (low energy).
• t≈2.0−2.5 s: First water hammer, vertical yellow band at x≈1.7−3.0 m.
• t>2.5 s: Periodically repeated structure of yellow bands with an interval of ~0.4 s → cyclic water hammer at a frequency of 2.39 Hz.

Wave propagation:

The diagonal orientation of energy features (blue-cyan transition zones) represents pressure wave propagation at effective speed c≈910 m/s.
Slope Δx/Δt≈900−1000 m/s confirms consistency with the FSI-reduced wave speed **[2,9].**

Key insight:

High-energy states (yellow) are highly **localised in space** (Δx≈1−2 m) and **time** (Δt≈0.002−0.010 s), validating the impulse concentration mechanism. Between events, the system returns to a low-energy continuous flow (violet-blue background level), demonstrating a clear spatio-temporal separation between discrete energy events.

Fig. 7. Volumetric energy density ε(t) at point A5 (control/drain branch outlet).

Discrete ejections of small control modules:

- **Startup control module** (t≈1.5 s):

ε*peak*≈2.38 MJ/m^3, volume 0.12 L, total energy 0.29 kJ. Fully dissipated through spring damper (15), Laval throttle nozzle (16) and hydraulic seal (6).

- **Transitional module** (t≈2.0 s):

ε*peak*≈2.0 MJ/m^3 with secondary oscillation. Represents intermediate ejection during acceleration from startup (2.66 m/s) to nominal velocity (13.42 m/s).

- **First nominal control module** (t≈2.62 s):

εpeak=10.061MJ/m^3, volume 0.26 L, ejection velocity 28.1 m/s, total energy **3.29 kJ**. Fully dissipated.

- **Subsequent nominal modules** (t≈3.04, 3.45 s):

Identical parameters to first nominal module – stable, repeating pattern confirms self-modulating operation.

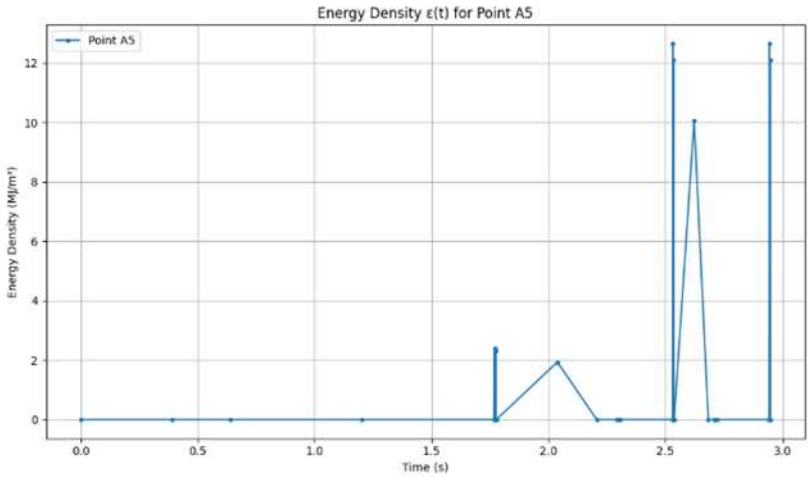

Energy dissipation mechanism (all control module energy intentionally sacrificed):

- Spring damper (15): absorbs ~30% of kinetic energy → heat.

- The Laval-type throttling nozzle (16): provides a sharp flow throttling (contraction–expansion), causing turbulent losses, jet separation, and cavitation, which effectively dissipates the velocity and removes ~50% of the energy.
- Hydraulic seal (6): final pressure drop to atmosphere, dissipates remaining ~20%.

Functional significance:
Although the control branch handles only **0.18% of total flow volume** (0.26 L vs. 141.3 L main module), it serves critical system functions:
1. Precise timing: V4 closure instant determines module formation synchronisation.
2. Air ingress prevention: Maintains hydraulic seal at bifurcation node during rarefaction (p=−0.8 atm).
3. Cycle overlap enabling: Allows next cycle to begin while previous module is still in transit, achieving 36% phase overlap.

Energy efficiency note:
Control branch dissipates 3.29 kJ per nominal cycle vs. 1,125.5 kJ delivered through main branch – **0.29% functional overhead**. This tiny cost is an acceptable trade-off for achieving stable self-modulating operation without external control systems.
Between control module ejections, ε=0at point A5 (no liquid present), confirming **complete hydraulic isolation** between control and delivery branches after bifurcation at A3.

Fig. 8. Volumetric energy density ε(t) at point A1 (supply pipeline upstream of valve V2).

Observed energy pulses:
- **Startup pulse** (t≈1.9−2.1 s):

ε*peak*≈2.32 MJ/m^3, P≈23.9 atm abs.. Extended plateau (Δt≈0.2 s) – reflects finite length of supply pipeline (L1=1.7 m) and pressure wave reflection dynamics [5].
- **First nominal pulse** (t≈2.4−2.6 s):

ε*peak*≈12.15 MJ/m^3, P=120.0 atm abs.. Sharp rising edge followed by sustained plateau (Δt≈0.15 s) – reflected water-hammer wave from V2 closure (t=2.535 s).
- **Second nominal pulse** (t≈2.9−3.2 s):Identical parameters – confirms stable, repeating nominal cycle operation.

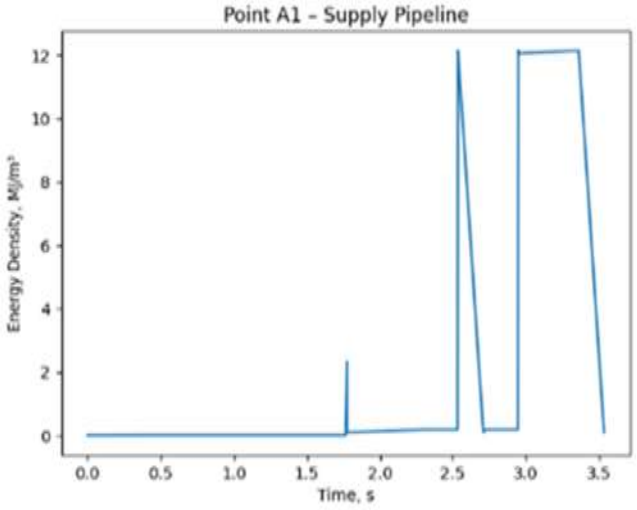

Spring damper (17) performance:
After each water-hammer peak, the damper reduces pressure from P*peak*=120.0 atm to P*residual*=1.887 atm within Δt≈0.05 s:

$$\eta damping = \frac{Ppeak - Presidual}{Ppeak} = \frac{120.0 - 1.887}{120.0} \approx 98.4\%.$$

Two critical functions of damping:

- **Backflow prevention:** Residual pressure (1.887 atm) is sufficient to prevent reverse flow into reservoir R1, maintaining unidirectional operation.
- **Rarefaction gradient establishment:** Damped pressure at A1 (1.887 atm) combined with rarefaction at A3 (−0.8 atm) creates ΔP=2.7 atm, which performs **38.5 kJ** of recuperative work per cycle (Section 3.3).

Plateau-shaped profile explanation:

The extended duration of high-energy states at A1 ($\Delta t \approx 0.15-0.20$ s, much longer than the theoretical water-hammer duration ~2 ms) results from:

- **Spatial averaging:** point A1 is embedded within a pipeline section of finite length (L1=1.7 m), experiencing pressure wave reflection between R1 and V2.
- **Spring damper response time:** finite compliance → gradual pressure decay.
- **Multiple wave reflections:** pressure oscillations between V2 and the damper create a sustained elevated pressure state before final dissipation [2,18].

Functional role:

Point A1 acts as an **elastic energy buffer** (though the stored energy is negligible, Section 2.4) and **pressure reference** that:

- Protects reservoir R1 from high-pressure transients.
- Maintains baseline pressure for continuous gravitational flow between cycles.
- Provides the high-pressure side of the recuperative gradient with A3.

Between nominal pulses, ε returns to baseline ($\varepsilon \approx 0.09$ MJ/m^3, 1.887 atm), which confirms the completeness of each cycle with full pressure reset.

Comparison with A3:

Unlike A3 (which experiences rarefaction, $\varepsilon<0$), point A1 never drops below atmospheric pressure due to the protective function of the spring damper and one-way valve V2. This demonstrates successful hydraulic isolation: the rarefaction-driven acceleration mechanism operates exclusively downstream of V2, while the supply pipeline maintains stable positive pressure.

Fig. 9. Evolution of the energy concentration ratio KEP as a function of Karney's ϕ-index from startup to nominal operation.

- Blue dashed curve: theoretical dependence **$KEP \propto \phi/(1-\phi)$** derived for impulse-dominated accumulative transient systems [11].
- Orange point: startup cycle.

$\phi start = H max,start / (H max,start + D cycle,start) = 327.8 / (327.8+66.7) = 0.831.$

KEPstart=167.

- Red point: nominal cycle.

$\phi nom = 1704/(1704+581.8) = 0.745.$

KEPcycle=574.

- Dotted line: system evolutionary trajectory from startup to stable nominal operation.

Interpretation:

- Both points lie in the accumulative regime ($\phi>0.5$), where the energy temporarily residing as enthalpy (pressure × volume) dominates over dissipation.
- The observed increase in KEP from 167 to 574 is not due to energy generation or efficiency improvement, but to the redistribution of energy in time and space:

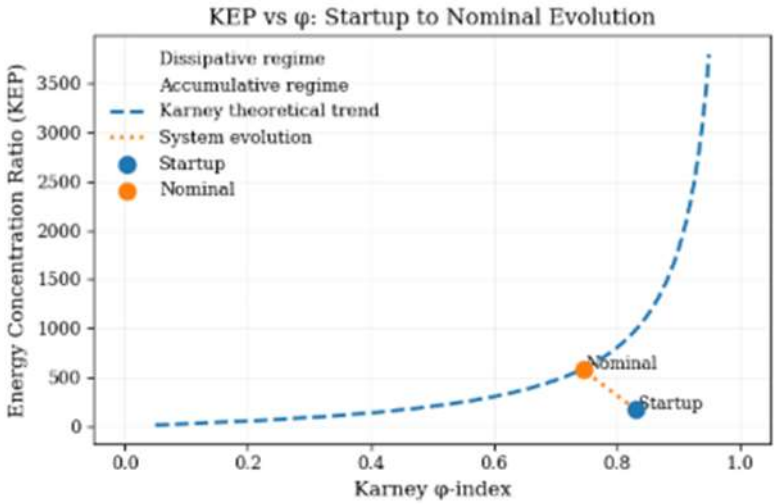

- Pre-acceleration caused by rarefaction (provided by internal energy recovery).
- A higher τ_acc/τ_dis ratio (effectively shorter dissipation time and faster pulse formation in nominal cycles).
- Stable self-regulation that reduces the influence of startup transients.

Quantitative validation of Karney's scaling [11]:

$$\mathbf{KEP}_{pred} = \frac{\tau_{acc}}{\tau_{dis}} \cdot \frac{\phi}{1-\phi} = \frac{0.4}{0.002} \cdot \frac{0.745}{0.255} = 200 \cdot 2.922 = 584.$$

Observed $KEP_{cycle}=574$ → error < 2%. This excellent agreement confirms that the GIF² system is a classical example of an accumulative transient system and that its performance is fully captured by Karney's energy framework without any hypothetical "elastic buffering" mechanisms.

Fig. 10. Evolution of energy conversion efficiency η as a function of Karney's ϕ-index from startup to nominal operation.

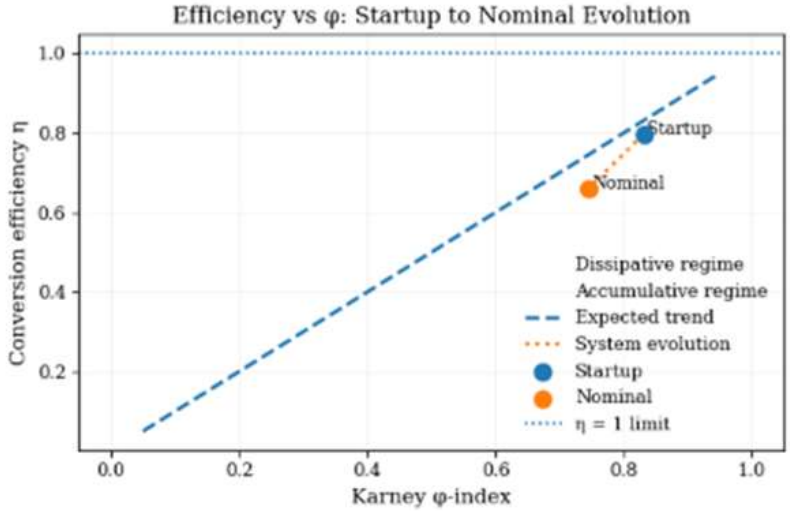

Green dashed line: expected trend – conversion efficiency generally increases with ϕ in purely dissipative systems [11].

- Orange point: startup cycle.

$\phi_{start}=0.831$, $\eta_{start}=H_{del,start}/H_{max,start}=261.4/327.8=0.797$.

- Red point: nominal cycle.

ϕ_{nom}=0.745, η_{nom}=1125.5/1704=0.661.

- Dashed trajectory: controlled transition toward stable operating regime.

Interpretation of the efficiency reduction (79.7% → 66.1%):

This reduction is design-driven and reflects the redistribution of enthalpy to maintain cyclic self-regulation:

- **Startup cycle:** no energy is "reserved" for the next cycle; almost all available enthalpy is converted to delivered work. However, the system cannot maintain this mode – without rarefaction pre-acceleration, the subsequent cycle would have much lower velocity and energy.
- **Nominal cycle:** 38.5 kJ per cycle is internally recuperated via the rarefaction to pre-accelerate the next cycle. This energy is temporarily "borrowed" from the current module and is not delivered at A9, thus reducing the apparent conversion efficiency.
- **Additionally:** 3.29 kJ per cycle is sacrificed in the control branch for timing and isolation – another deliberate efficiency reduction for functional gain.

Thus the lower η at higher ϕ is not a paradox; it is a design choice. The system trades part of its instantaneous conversion efficiency for cycle stability (self-oscillating mode), higher KEP, and a quasi-continuous output signal.

All efficiency values remain below unity, confirming strict adherence to energy conservation.

APPENDIX A.5. TIME-DOMAIN ENERGY DATA AT CONTROL POINTS

Pressure (absolute), velocity, and volumetric mechanical energy density $\varepsilon=(p-p_{atm})+\frac{1}{2}\rho v^2$ for startup and nominal cycles.

General notes for Tables A.5.1–A.5.4:

- Pressure p is given in **absolute atmospheres** (atm abs.).

Atmospheric pressure patm=1 atm=101325 Pa.

- Volumetric energy density ε(t) is calculated as

$\varepsilon=(p-1)\times 101325+500\cdot v^2$[J/m3], where $\mathbf{500=\frac{1}{2}\rho}$ with ρ=1000 kg/m^3.

- This **ε** represents the specific mechanical work potential (enthalpy difference + kinetic energy) per unit volume **[22, 23].**

When multiplied by the volume of a coherent liquid module, **ε·V** gives the total mechanical work that the module would deliver if expanded isobarically to atmospheric pressure and brought to rest.

- When the liquid phase is absent (cell «no water»), the pressure is atmospheric (1.0 atm abs.) and ε = 0; the flow velocity is undefined and set to zero for the calculation.
- Main module volume (working pipeline 3): V_module = 0.1413 m³.

Small control module volume (drain pipeline 5): startup 0.12 L, nominal 0.26 L..

- True elastic energy (liquid compression + pipe-wall strain) is evaluated separately in Section 2.4 and amounts to less than 0.8% of H_max; it is not included in ε.

- **Table A.5.1** – **Point A1** (supply pipeline, upstream of valve V2). Pressure p(t), Velocity v(t) and Volumetric energy density ε(t) at Point A1 of Supply Inclined Pipeline 1 (0.55 m gravitational height from point B before valve-interrupter 2) in startup and nominal GIF² cycles.

- **Table A.5.2** – **Point A3** (working pipeline, bifurcation node). Pressure p(t), Velocity v(t) and Volumetric energy density ε(t) at point A3 – working pipeline 3 (1.5 m downstream of valve V2, 1.5 m upstream of impact valve V4) in startup and nominal GIF² cycles.

• **Table A.5.3** – **Point A9** (delivery branch outlet). Pressure p(t), Velocity v(t) and Volumetric energy density ε(t) at Point A9 of Discharge Pipeline 9 (After transit hydraulic accumulator-pressure stabilizer or 0.376 m from nozzle exit) in startup and nominal GIF² cycles..

• **Table A.5.4** – Point A5 (control/drain branch outlet). Pressure p(t), flow Velocity v(t) and Volumetric energy density ε(t) at point A5 of drain pipeline 5 (located 3 meters from the axis of the shock valve 4 disc, upstream of the spring-type hydraulic impulse damper (15) for small impulse-module pressure amplitude in drain pipeline (5) — atmospheric discharge with complete dissipation through Laval throttle nozzle 16 and hydraulic seal 6 of the GIF² system).

Note: The rarefaction pressure of –0.8 atm gauge (0.2 atm absolute) is stably reproduced in each nominal cycle. A negative ε indicates that the fluid is in tension; work must be done on the fluid to return it to atmospheric conditions.

GIF² (Gravity Impulse Flow Former) System Control Points

Table A.5.1: Point A1 (supply pipeline, upstream of valve V2)

Time, s	p(t), atm	v(t), m/s	ε(t), J/m³	Calculation ε(t), (J/m³) ε(t) = ΔP(t) + ρ·v(t)²/2 = (P(t)-1)×101325 + 500·v(t)²	Note
0	1.0	0	0	(1-1)×101325 + 500×0²	Start of continuous flow of 222.1 L from reservoir R1 through pipeline 1.
0.3906	1.034	2.66 ↓	6 981	(1.034-1)×101325 + 500×2.66²	Continuous flow 222.1 L at point A1 of pipeline 1.
0.639	1.034	2.66	6 981	(1.034-1)×101325 + 500×2.66²	Continuous flow 222.1 L at point B (valve 2) of pipeline 3. P(t)=0.087
1.203	1.034	2.66	6 981	(1.034-1)×101325 + 500×2.66²	Continuous flow 222.1 L at control point A3 of pipeline 3 before valve 4. P(t)=0.087
1.766917	1.034	2.66 ↓	6 981	(1.034-1)×101325 + 500×2.66²	Continuous flow 222.1 L before hydraulic shock at valve 4. Disc closing time (0.00303 s).
1.769947	1.034	2.66	6 981	(1.034-1)×101325 + 500×2.66²	Hydraulic shock at valve 4. Pressure amplitude 23.9 atm. First flow interruption. Formation of small module (0) in drain pipeline 5: Startup cycle: volume = 0.12 L, ejection speed = 11.2 m/s. Module is discharged to atmosphere through spring damper 15, Laval nozzle 16 and hydraulic seal 6 (L5 = 4.7 m). Flow deceleration and stop. Opening of valve 7 disc.
1.771596	1.034	2.66	6 981	(1.034-1)×101325 + 500×2.66²	Shock wave front (0.0016483 s) at control point A3.
1.7732437	1.034	2.66	6 981	(1.034-1)×101325 + 500×2.66²	Shock wave front from valve 4 disc reaches valve 2 disc (0.0032967 s).
1.7749537	1.034	2.66	6 981	(1.034-1)×101325 + 500×2.66²	Hydraulic shock at valve 2. Disc closing time 0.00171 s. Second flow interruption. Formation of module (0) 141.3 L in pipeline 3. Start of module (0) motion in pipeline 3 (L3=3 m; v=5.8 m/s).
1.7756797	23.9	0	2 320 343	(23.9-1)×101325 + 500×0²	Shock wave front (0.000726 s) from valve 2 disc reaches control point A1. Passage of shock wave front to spring hydraulic pulse pressure amplitude damper (17) in supply pipeline (1) and to the second bottom of reservoir R1. Flow deceleration of 222.1 L in pipeline 1.
1.7771515	1.887	0	89 875	(1.887-1)×101325 + 500×0²	Shock wave front (0.0021978 s) from valve 2 disc reaches the second bottom of reservoir R1, damped to pressure 1.887 atm. Flow in pipeline (1) stopped. Valve 2 closed.
2.2921947	1.887	0	89 875	(1.887-1)×101325 + 500×0²	Module (0) moved into pipeline 9 through valve 7 (0.517241 s), module speed 5.6 m/s, pressure 19.6 atm).
2.2974147	1.887	0	89 875	(1.887-1)×101325 + 500×0²	Closing of valve 7 disc. Closing time 0.00522 s. Vacuum phase in pipeline 3 (-0.8 atm). Flow in pipeline (1) stopped. Opening of valve 2 (0.008896 s). Start of nominal cycle (1).
2.3063107	1.887	13.42	179 957	(1.887-1)×101325 + 500×13.42²	Valve 2 disc opened. Resumption of continuous flow in pipelines 1 and 3. Continuous flow 13.42 m/s restored. Travel time to valve 4: 0.223547 s.
2.529858	1.887	13.42	179 957	(1.887-1)×101325 + 500×13.42²	Continuous flow near valve 4 disc. Disc closing. Closing time 0.00134 s.
2.531198	1.887	13.42	179 957	(1.887-1)×101325 + 500×13.42²	Hydraulic shock at valve 4. Pressure amplitude 120.5 atm. First flow interruption. Flow deceleration and stop. Formation of small module (1) in drain pipeline 5: Nominal cycle: volume = 0.26 L, ejection speed = 32.8 m/s. Module is discharged to atmosphere through spring damper 15, Laval nozzle 16 and hydraulic seal 6 (L5 = 4.7 m). Opening of valve 7 disc.
2.5328463	1.887	13.42	179 957	(1.887-1)×101325 + 500×13.42²	Shock wave front (0.0016483 s) at control point A3.
2.5344947	1.887	13.42	179 957	(1.887-1)×101325 + 500×13.42²	Shock wave front from valve 4 disc reaches valve 2 disc (0.0032967 s).
2.5352597	1.887	13.42	179 957	(1.887-1)×101325 + 500×13.42²	Hydraulic shock at valve 2. Disc closing time 0.000765 s. Pressure amplitude 120 atm. Second flow interruption. Formation of module (1) 141.3 L in pipeline 3. Start of module (1) motion in pipeline 3 (L3=3 m; v=17.3 m/s).
2.5359857	120	0	12 057 675	(120-1)×101325 + 500×0²	Shock wave front (0.000726 s) from valve 2 disc reaches control point A1. Passage of shock wave front to spring hydraulic pulse pressure amplitude damper (17) in supply pipeline (1) and to the second bottom of reservoir R1. Flow deceleration of 222.1 L in pipeline 1.
2.5374575	1.887	0	89 875	(1.887-1)×101325 + 500×0²	Shock wave front (0.0021978 s) from valve 2 disc reaches the second bottom of reservoir R1, damped to pressure 1.887 atm. Flow in pipeline (1) stopped. Valve 2 closed.
2.7086697	1.887	0	89 875	(1.887-1)×101325 + 500×0²	Module (1) moved into pipeline 9 through valve 7 (0.17341 s), module speed 15.1 m/s, pressure 96.4 atm).
2.7110897	1.887	0	89 875	(1.887-1)×101325 + 500×0²	Closing of valve 7 disc. Closing time 0.00242 s. Vacuum phase in pipeline 3 (-0.8 atm). Flow in pipeline (1) stopped. Opening of valve 2 (0.008896 s). Start of nominal cycle (2).
2.7199857	1.887	13.42	179 957	(1.887-1)×101325 + 500×13.42²	Valve 2 disc opened. Resumption of continuous flow in pipelines 1 and 3. Continuous flow 13.42 m/s restored. Travel time to valve 4 (0.223547 s).
2.9435327	1.887	13.42	179 957	(1.887-1)×101325 + 500×13.42²	Continuous flow near valve 4 disc. Disc closing. Closing time 0.00134 s.

Time, s	p(t), atm	v(t), m/s	ε(t), J/m³	Calculation ε(t), (J/m³) ε(t) = ΔP(t) + ρ·v(t)²/2 = (P(t)-1)×101325 + 500·v(t)²	Note
2.9448727	1.887	13.42	179 957	(1.887-1)×101325 + 500×13.42²	Hydraulic shock at valve 4. Pressure amplitude 120.5 atm. First flow interruption. Flow deceleration and stop. Formation of small module (2) in drain pipeline 5: Nominal cycle: volume = 0.26 L, ejection speed = 32.8 m/s. Module is discharged to atmosphere through spring damper 15, Laval nozzle 16 and hydraulic seal 6 (L5 = 4.7 m). Opening of valve 7 disc.
2.9465210	1.887	13.42	179 957	(1.887-1)×101325 + 500×13.42²	Shock wave front (0.0016483 s) at control point A3.
2.9481694	1.887	13.42	179 957	(1.887-1)×101325 + 500×13.42²	Shock wave front from valve 4 disc reaches valve 2 disc (0.0032967 s).
2.9489344	1.887	13.42	179 957	(1.887-1)×101325 + 500×13.42²	Hydraulic shock at valve 2. Disc closing time 0.000765 s. Pressure amplitude 120 atm. Second flow interruption. Formation of module (2) 141.3 L in pipeline 3. Start of module (2) motion in pipeline 3 (L3=3 m; v=17.3 m/s).
2.9496604	120	0	12 057 675	(120-1)×101325 + 500×0²	Shock wave front (0.000726 s) from valve 2 disc reaches control point A1. Passage of shock wave front to spring hydraulic pulse pressure amplitude damper (17) in supply pipeline (1) and to the second bottom of reservoir R1. Flow deceleration of 222.1 L in pipeline 1.
2.9511322	1.887	0	89 875	(1.887-1)×101325 + 500×0²	Shock wave front (0.0021978 s) from valve 2 disc reaches the second bottom of reservoir R1, damped to pressure 1.887 atm. Flow in pipeline (1) stopped. Valve 2 closed.
2.9528947	1.887	0	89 875	(1.887-1)×101325 + 500×0²	Completion of module (0) motion through pipeline 9 (3.7 m) to nozzle (0.6607 s, speed 5.6 m/s, pressure 19.1 atm). End of startup cycle (0).
2.9537027	1.887	0	89 875	(1.887-1)×101325 + 500×0²	Completion of module (1) motion through pipeline 9 (3.7 m) to nozzle (0.245033 s, speed 15.1 m/s, pressure 78.48 atm). End of nominal cycle (1).
3.1223444	1.887	0	89 875	(1.887-1)×101325 + 500×0²	Module (2) moved into pipeline 9 through valve 7 (0.17341 s), module speed 15.1 m/s, pressure 96.4 atm).
3.1247644	1.887	0	89 875	(1.887-1)×101325 + 500×0²	Closing of valve 7 disc. Closing time 0.00242 s. Vacuum phase in pipeline 3 (-0.8 atm). Flow in pipeline (1) stopped. Opening of valve 2 (0.008896 s). Start of nominal cycle (3).
3.1336604	1.887	13.42	179 957	(1.887-1)×101325 + 500×13.42²	Valve 2 disc opened. Resumption of continuous flow in pipelines 1 and 3. Continuous flow 13.42 m/s restored. Travel time to valve 4 (0.223547 s).
3.3572074	1.887	13.42	179 957	(1.887-1)×101325 + 500×13.42²	Continuous flow near valve 4 disc. Disc closing. Closing time 0.00134 s.
3.3585474	1.887	13.42	179 957	(1.887-1)×101325 + 500×13.42²	Hydraulic shock at valve 4. Pressure amplitude 120.5 atm. First flow interruption. Flow deceleration and stop. Formation of small module (3) in drain pipeline 5: Nominal cycle: volume = 0.26 L, ejection speed = 32.8 m/s. Module is discharged to atmosphere through spring damper 15, Laval nozzle 16 and hydraulic seal 6 (L5 = 4.7 m). Opening of valve 7 disc.
3.3601957	1.887	13.42	179 957	(1.887-1)×101325 + 500×13.42²	Shock wave front (0.0016483 s) at control point A3.
3.3618441	1.887	13.42	179 957	(1.887-1)×101325 + 500×13.42²	Shock wave front from valve 4 disc reaches valve 2 disc (0.0032967 s).
3.3626091	1.887	13.42	179 957	(1.887-1)×101325 + 500×13.42²	Hydraulic shock at valve 2. Disc closing time 0.000765 s. Pressure amplitude 120 atm. Second flow interruption. Formation of module (3) 141.3 L in pipeline 3. Start of module (3) motion in pipeline 3 (L3=3 m; v=17.3 m/s).
3.3633351	120	0	12 057 675	(120-1)×101325 + 500×0²	Shock wave front (0.000726 s) from valve 2 disc reaches control point A1. Passage of shock wave front to spring hydraulic pulse pressure amplitude damper (17) in supply pipeline (1) and to the second bottom of reservoir R1. Flow deceleration of 222.1 L in pipeline 1.
3.3648069	1.887	0	89 875	(1.887-1)×101325 + 500×0²	Shock wave front (0.0021978 s) from valve 2 disc reaches the second bottom of reservoir R1, damped to pressure 1.887 atm. Flow in pipeline (1) stopped. Valve 2 closed.
3.3673774	1.887	0	89 875	(1.887-1)×101325 + 500×0²	Completion of module (2) motion through pipeline 9 (3.7 m) to nozzle (0.245033 s, speed 15.1 m/s, pressure 78.48 atm). End of nominal cycle (2).
3.5360191	1.887	0	89 875	(1.887-1)×101325 + 500×0²	Module (3) moved into pipeline 9 through valve 7 (0.17341 s), module speed 15.1 m/s, pressure 96.4 atm).

Table A.5.2 – Point A3 (working pipeline, bifurcation node).

Time, s	p(t), atm	v(t), m/s	ε(t), J/m³	Calculation ε(t), (J/m³) ε(t) = ΔP(t) + ρ·v(t)²/2 = (P(t)-1)×101325 + 500·v(t)²	Note
0	1.0	0	0	(1-1)×101325 + 500×0²	Start of continuous flow of 222.1 L from reservoir R1 through pipeline 1.
0.3906	1.0	–	0	(1-1)×101325 + 500×0²	no water. Continuous flow 222.1 L at point A1 of pipeline 1.
0.639	1.087	2.66	12 352	(1.087-1)×101325 + 500×2.66²	no water. Continuous flow 222.1 L at point B (valve 2) of pipeline 3.
1.203	1.087	2.66	12 352	(1.087-1)×101325 + 500×2.66²	Continuous flow 222.1 L at control point A3 of pipeline 3 before valve 4.

1.766917	1.087	2.66 ↓	12 352	(1.087-1)×101325 + 500×2.66²	Continuous flow 222.1 L before hydraulic shock at valve 4. Disc closing time (0.00303 s).
1.769947	1.087	2.66	12 352	(1.087-1)×101325 + 500×2.66²	Hydraulic shock at valve 4. Pressure amplitude 23.9 atm. First flow interruption. Formation of small module (0) in drain pipeline 5: Startup cycle: volume = 0.12 L, ejection speed = 11.2 m/s. Module is discharged to atmosphere through spring damper 15, Laval nozzle 16 and hydraulic seal 6 (L5 = 4.7 m). Flow deceleration and stop. Opening of valve 7 disc.
1.771596	23.9	0	2 320 343	(23.9-1)×101325 + 500×0²	Shock wave front (0.0016483 s) at control point A3.
1.7732437	23.9	0	2 320 343	(23.9-1)×101325 + 500×0²	Shock wave front from valve 4 disc reaches valve 2 disc (0.0032967 s).
1.7749537	23.9	0	2 320 343	(23.9-1)×101325 + 500×0²	Hydraulic shock at valve 2. Disc closing time 0.00171 s. Second flow interruption. Formation of module (0) 141.3 L in pipeline 3. Start of module (0) motion in pipeline 3 (L3=3 m; v=5.8 m/s).
1.7756797	23.9	0	2 320 343	(23.9-1)×101325 + 500×0²	Shock wave front (0.000726 s) from valve 2 disc reaches control point A1. Passage of shock wave front to spring hydraulic pulse pressure amplitude damper (17) in supply pipeline (1) and to the second bottom of reservoir R1. Flow deceleration of 222.1 L in pipeline 1.
1.7771515	23.9	0	2 320 343	(23.9-1)×101325 + 500×0²	Shock wave front (0.0021978 s) from valve 2 disc reaches the second bottom of reservoir R1, damped to pressure 1.887 atm. Flow in pipeline (1) stopped. Valve 2 closed.
2.2921947	19.6	5.8	1 896 000	(19.6-1)×101325 + 500×5.8²	Module (0) moved into pipeline 9 through valve 7 (0.517241 s), module speed 5.6 m/s, pressure 19.6 atm).
2.2974147	-0.8	–	-182 385	(-0.8-1)×101325 + 500×0²	no water. Closing of valve 7 disc. Closing time 0.00522 s. Vacuum phase in pipeline 3 (-0.8 atm). Flow in pipeline (1) stopped. Opening of valve 2 (0.008896 s). Start of nominal cycle (1).
2.3063107	1.887	13.42	179 957	(1.887-1)×101325 + 500×13.42²	Valve 2 disc opened. Resumption of continuous flow in pipelines 1 and 3. Continuous flow 13.42 m/s restored. Travel time to valve 4: 0.223547 s.
2.529858	1.887	13.42	179 957	(1.887-1)×101325 + 500×13.42²	Continuous flow near valve 4 disc. Disc closing. Closing time 0.00134 s.
2.531198	1.887	13.42	179 957	(1.887-1)×101325 + 500×13.42²	Hydraulic shock at valve 4. Pressure amplitude 120.5 atm. First flow interruption. Flow deceleration and stop. Formation of small module (1) in drain pipeline 5: Nominal cycle: volume = 0.26 L, ejection speed = 32.8 m/s. Module is discharged to atmosphere through spring damper 15, Laval nozzle 16 and hydraulic seal 6 (L5 = 4.7 m). Opening of valve 7 disc.
2.5328463	120.5	0	12 108 338	(120.5-1)×101325 + 500×0²	Shock wave front (0.0016483 s) at control point A3.
2.5344947	120.5	0	12 108 338	(120.5-1)×101325 + 500×0²	Shock wave front from valve 4 disc reaches valve 2 disc (0.0032967 s).
2.5352597	120	0	12 057 675	(120-1)×101325 + 500×0²	Hydraulic shock at valve 2. Disc closing time 0.000765 s. Pressure amplitude 120 atm. Second flow interruption. Formation of module (1) 141.3 L in pipeline 3. Start of module (1) motion in pipeline 3 (L3=3 m; v=17.3 m/s).
2.5359857	120	0	12 057 675	(120-1)×101325 + 500×0²	Shock wave front (0.000726 s) from valve 2 disc reaches control point A1. Passage of shock wave front to spring hydraulic pulse pressure amplitude damper (17) in supply pipeline (1) and to the second bottom of reservoir R1. Flow deceleration of 222.1 L in pipeline 1.
2.5374575	120	0	12 057 675	(120-1)×101325 + 500×0²	Shock wave front (0.0021978 s) from valve 2 disc reaches the second bottom of reservoir R1, damped to pressure 1.887 atm. Flow in pipeline (1) stopped. Valve 2 closed.
2.7086697	96.4	17.3	9 815 768	(96.4-1)×101325 + 500×17.3²	Module (1) moved into pipeline 9 through valve 7 (0.17341 s), module speed 15.1 m/s, pressure 96.4 atm).
2.7110897	-0.8	–	-182 385	(-0.8-1)×101325 + 500×0²	no water. Closing of valve 7 disc. Closing time 0.00242 s. Vacuum phase in pipeline 3 (-0.8 atm). Flow in pipeline (1) stopped. Opening of valve 2 (0.008896 s). Start of nominal cycle (2).
2.7199857	1.887	13.42	179 957	(1.887-1)×101325 + 500×13.42²	Valve 2 disc opened. Resumption of continuous flow in pipelines 1 and 3. Continuous flow 13.42 m/s restored. Travel time to valve 4 (0.223547 s).
2.9435327	1.887	13.42	179 957	(1.887-1)×101325 + 500×13.42²	Continuous flow near valve 4 disc. Disc closing. Closing time 0.00134 s.
2.9448727	1.887	13.42	179 957	(1.887-1)×101325 + 500×13.42²	Hydraulic shock at valve 4. Pressure amplitude 120.5 atm. First flow interruption. Flow deceleration and stop. Formation of small module (2) in drain pipeline 5: Nominal cycle: volume = 0.26 L, ejection speed = 32.8 m/s. Module is discharged to atmosphere through spring damper 15, Laval nozzle 16 and hydraulic seal 6 (L5 = 4.7 m). Opening of valve 7 disc.
2.9465210	120.5	0	12 108 338	(120.5-1)×101325 + 500×0²	Shock wave front (0.0016483 s) at control point A3.
2.9481694	120.5	0	12 108 338	(120.5-1)×101325 + 500×0²	Shock wave front from valve 4 disc reaches valve 2 disc (0.0032967 s).
2.9489344	120	0	12 057 675	(120-1)×101325 + 500×0²	Hydraulic shock at valve 2. Disc closing time 0.000765 s. Pressure amplitude 120 atm. Second flow interruption. Formation of module (2) 141.3 L in pipeline 3. Start of module (2) motion in pipeline 3 (L3=3 m; v=17.3 m/s).
2.9496604	120	0	12 057 675	(120-1)×101325 + 500×0²	Shock wave front (0.000726 s) from valve 2 disc reaches control point A1. Passage of shock wave front to spring hydraulic pulse pressure amplitude damper (17) in supply pipeline (1) and to the second bottom of reservoir R1. Flow deceleration of 222.1 L in pipeline 1.
2.9511322	1.887	0	89 875	(1.887-1)×101325 + 500×0²	Shock wave front (0.0021978 s) from valve 2 disc reaches the second bottom of reservoir R1, damped to pressure 1.887 atm. Flow in pipeline (1) stopped. Valve 2 closed.
2.9528947	1.887	13.42	179 957	(1.887-1)×101325 + 500×13.42²	Completion of module (0) motion through pipeline 9 (3.7 m) to nozzle (0.6607 s, speed 5.6 m/s, pressure 19.1 atm). End of startup cycle

					(0).
2.9537027	120	0	12 057 675	(120-1)×101325 + 500×0²	Completion of module (1) motion through pipeline 9 (3.7 m) to nozzle (0.245033 s, speed 15.1 m/s, after pressure stabilization to 78.48 atm). End of nominal cycle (1).
3.1223444	96.4	17.3	9 815 768	(96.4-1)×101325 + 500×17.3²	Module (2) moved into pipeline 9 through valve 7 (0.17341 s), module speed 15.1 m/s, pressure 96.4 atm).
3.1247644	-0.8	–	-182 385	(-0.8-1)×101325 + 500×0²	no water. Closing of valve 7 disc. Closing time 0.00242 s. Vacuum phase in pipeline 3 (-0.8 atm). Flow in pipeline (1) stopped. Opening of valve 2 (0.008896 s). Start of nominal cycle (3).
3.1336604	1.887	13.42	179 957	(1.887-1)×101325 + 500×13.42²	Valve 2 disc opened. Resumption of continuous flow in pipelines 1 and 3. Continuous flow 13.42 m/s restored. Travel time to valve 4 (0.223547 s).
3.3572074	1.887	13.42	179 957	(1.887-1)×101325 + 500×13.42²	Continuous flow near valve 4 disc. Disc closing. Closing time 0.00134 s.
3.3585474	1.887	13.42	179 957	(1.887-1)×101325 + 500×13.42²	Hydraulic shock at valve 4. Pressure amplitude 120.5 atm. First flow interruption. Flow deceleration and stop. Formation of small module (3) in drain pipeline 5: Nominal cycle: volume = 0.26 L, ejection speed = 32.8 m/s. Module is discharged to atmosphere through spring damper 15, Laval nozzle 16 and hydraulic seal 6 (L5 = 4.7 m). Opening of valve 7 disc.
3.3601957	120.5	0	12 108 338	(120.5-1)×101325 + 500×0²	Shock wave front (0.0016483 s) at control point A3.
3.3618441	120.5	0	12 108 338	(120.5-1)×101325 + 500×0²	Shock wave front from valve 4 disc reaches valve 2 disc (0.0032967 s).
3.3626091	120	0	12 057 675	(120-1)×101325 + 500×0²	Hydraulic shock at valve 2. Disc closing time 0.000765 s. Pressure amplitude 120 atm. Second flow interruption. Formation of module (3) 141.3 L in pipeline 3. Start of module (3) motion in pipeline 3 (L3=3 m; v=17.3 m/s).
3.3633351	120	0	12 057 675	(120-1)×101325 + 500×0²	Shock wave front (0.000726 s) from valve 2 disc reaches control point A1. Passage of shock wave front to spring hydraulic pulse pressure amplitude damper (17) in supply pipeline (1) and to the second bottom of reservoir R1. Flow deceleration of 222.1 L in pipeline 1.
3.3648069	1.887	0	89 875	(1.887-1)×101325 + 500×0²	Shock wave front (0.0021978 s) from valve 2 disc reaches the second bottom of reservoir R1, damped to pressure 1.887 atm. Flow in pipeline (1) stopped. Valve 2 closed.
3.3673774	120	0	12 057 675	(120-1)×101325 + 500×0²	Completion of module (2) motion through pipeline 9 (3.7 m) to nozzle (0.245033 s, speed 15.1 m/s, pressure 78.48 atm stabilized). End of nominal cycle (2).
3.5360191	96.4	17.3	9 815 768	(96.4-1)×101325 + 500×17.3²	Module (3) moved into pipeline 9 through valve 7 (0.17341 s), module speed 15.1 m/s, pressure 96.4 atm).

Table A.5.3 – Point **A9** (delivery branch outlet).

Time, s	**p(t), atm**	**v(t), m/s**	**ε(t), J/m³**	**Calculation ε(t), (J/m³) ε(t) = ΔP(t) + ρ·v(t)²/2 = (P(t)-1)×101325 + 500·v(t)²**	**Note**
0	1.0	–	0	(1-1)×101325 + 500×0²	Start of continuous flow of 222.1 L from reservoir R1 through pipeline 1.
0.3906	1.0	–	0	(1-1)×101325 + 500×0²	no water. Continuous flow 222.1 L at point A1 of pipeline 1.
0.639	1.0	–	0	(1-1)×101325 + 500×0²	no water. Continuous flow 222.1 L at point B (valve 2) of pipeline 3.
1.203	1.0	–	0	(1-1)×101325 + 500×0²	no water. Continuous flow 222.1 L at control point A3 of pipeline 3 before valve 4.
1.766917	1.0	–	0	(1-1)×101325 + 500×0²	no water. Continuous flow 222.1 L before hydraulic shock at valve 4. Disc closing time (0.00303 s).
1.769947	1.0	–	0	(1-1)×101325 + 500×0²	Hydraulic shock at valve 4. Pressure amplitude 23.9 atm. First flow interruption. Formation of small module (0) in drain pipeline 5: Startup cycle: volume = 0.12 L, ejection speed = 11.2 m/s. Module is discharged to atmosphere through spring damper 15, Laval nozzle 16 and hydraulic seal 6 (L5 = 4.7 m). Flow deceleration and stop. Opening of valve 7 disc.
1.771596	1.0	–	0	(1-1)×101325 + 500×0²	Shock wave front (0.0016483 s) at control point A3.
1.7732437	1.0	–	0	(1-1)×101325 + 500×0²	Shock wave front from valve 4 disc reaches valve 2 disc (0.0032967 s).
1.7749537	1.0	–	0	(1-1)×101325 + 500×0²	Hydraulic shock at valve 2. Disc closing time 0.00171 s. Second flow interruption. Formation of module (0) 141.3 L in pipeline 3. Start of module (0) motion in pipeline 3 (L3=3 m; v=5.8 m/s).
1.7756797	1.0	–	0	(1-1)×101325 + 500×0²	Shock wave front (0.000726 s) from valve 2 disc reaches control point A1. Passage of shock wave front to spring hydraulic pulse pressure amplitude damper (17) in supply pipeline (1) and to the second bottom of reservoir R1. Flow deceleration of 222.1 L in pipeline 1.
1.7771515	1.0	–	0	(1-1)×101325 + 500×0²	Shock wave front (0.0021978 s) from valve 2 disc reaches the second bottom of reservoir R1, damped to pressure 1.887 atm. Flow in pipeline (1) stopped. Valve 2 closed.
2.2921947	1.0	–	0	(1-1)×101325 + 500×0²	Module (0) moved into pipeline 9 through valve 7 (0.517241 s), module speed 5.6 m/s, 19.1 atm, module tail).
2.2974147	1.0	–	0	(1-1)×101325 + 500×0²	Closing of valve 7 disc. Closing time 0.00522 s. Vacuum phase in pipeline 3 (-0.8 atm). Flow in pipeline (1) stopped. Opening of valve 2

Time, s	p(t), atm	v(t), m/s	ε(t), J/m³	Calculation ε(t), (J/m³) ε(t) = ΔP(t) + ρ·v(t)²/2 = (P(t)-1)×101325 + 500·v(t)²	Note
					(0.008896 s). Start of nominal cycle (1).
2.3063107	1.0	–	0	(1-1)×101325 + 500×0²	Valve 2 disc opened. Resumption of continuous flow in pipelines 1 and 3. Continuous flow 13.42 m/s. Travel time to valve 4: 0.223547 s.
2.529858	1.0	–	0	(1-1)×101325 + 500×0²	Continuous flow near valve 4 disc. Disc closing (0.00134 s).
2.531198	1.0	–	0	(1-1)×101325 + 500×0²	Hydraulic shock at valve 4. Pressure amplitude 120.5 atm. First flow interruption. Flow deceleration and stop. Formation of small module (1) in drain pipeline 5: Nominal cycle: volume = 0.26 L, ejection speed = 32.8 m/s. Module is discharged to atmosphere through spring damper 15, Laval nozzle 16 and hydraulic seal 6 (L5 = 4.7 m). Opening of valve 7 disc.
2.5328463	1.0	–	0	(1-1)×101325 + 500×0²	Shock wave front (0.0016483 s) at control point A3.
2.5344947	1.0	–	0	(1-1)×101325 + 500×0²	Shock wave front from valve 4 disc reaches valve 2 disc (0.0032967 s).
2.5352597	1.0	–	0	(1-1)×101325 + 500×0²	Hydraulic shock at valve 2. Disc closing time 0.000765 s. Pressure amplitude 120 atm. Second flow interruption. Formation of module (1) 141.3 L in pipeline (3). Start of module (1) motion in pipeline (3): (L3=3 m; v=17.3 m/s).
2.5359857	1.0	–	0	(1-1)×101325 + 500×0²	Shock wave front from valve 2 disc (0.661 m) reaches control point A1 (0.000726 s). Passage of shock wave front to spring hydraulic pulse pressure amplitude damper (17) in supply pipeline (1) and to the second bottom of reservoir R1. Flow deceleration of 222.1 L in pipeline 1.
2.5374575	1.0	–	0	(1-1)×101325 + 500×0²	Shock wave front (0.0021978 s) from valve 2 disc reaches the second bottom of reservoir R1, damped to pressure 1.887 atm. Flow in pipeline (1) stopped. Valve 2 closed.
2.7086697	1.0	–	0	(1-1)×101325 + 500×0²	Module (1) moved into pipeline 9 through valve 7 (0.17341 s), module speed 15.1 m/s, pressure 96.4 atm, module tail).
2.7110897	1.0	–	0	(1-1)×101325 + 500×0²	Closing of valve 7 disc. Closing time 0.00242 s. Vacuum phase in pipeline 3 (-0.8 atm). Flow in pipeline (1) stopped. Opening of valve 2 (0.008896 s). Start of nominal cycle (2).
2.7199857	1.0	–	0	(1-1)×101325 + 500×0²	Valve 2 disc opened. Resumption of continuous flow in pipelines 1 and 3. Continuous flow 13.42 m/s restored. Travel to valve 4 (0.223547 s).
2.9435327	1.0	–	0	(1-1)×101325 + 500×0²	Continuous flow near valve 4 disc. Disc closing, closing time 0.00134 s.
2.9448727	1.0	–	0	(1-1)×101325 + 500×0²	Hydraulic shock at valve 4. Pressure amplitude 120.5 atm. First flow interruption. Flow deceleration and stop. Formation of small module (2) in drain pipeline 5: Nominal cycle: volume = 0.26 L, ejection speed = 32.8 m/s. Module is discharged to atmosphere through spring damper 15, Laval nozzle 16 and hydraulic seal 6 (L5 = 4.7 m). Opening of valve 7 disc.
2.9465210	1.0	–	0	(1-1)×101325 + 500×0²	Shock wave front (0.0016483 s) at control point A3 (1.5 m).
2.9481694	1.0	–	0	(1-1)×101325 + 500×0²	Shock wave front from valve 4 disc reaches valve 2 disc (0.0032967 s), 3 m.
2.9489344	1.0	–	0	(1-1)×101325 + 500×0²	Hydraulic shock at valve 2. Disc closing time 0.000765 s. Pressure amplitude 120 atm. Second flow interruption. Formation of module (2) 141.3 L in pipeline 3. Start of module (2) motion in pipeline 3 (L3=3 m; v=17.3 m/s).
2.9496604	1.0	–	0	(1-1)×101325 + 500×0²	Shock wave front (0.000726 s) from valve 2 disc reaches control point A1. Passage of shock wave front to spring hydraulic pulse pressure amplitude damper (17) in supply pipeline (1) and to the second bottom of reservoir R1. Flow deceleration of 222.1 L in pipeline 1.
2.9511322	1.0	–	0	(1-1)×101325 + 500×0²	Shock wave front (0.0021978 s) from valve 2 disc reaches the second bottom of reservoir R1, damped to pressure 1.887 atm. Flow in pipeline (1) stopped. Valve 2 closed.
2.9528947	19.1	5.6	1 849 385	(19.1-1)×101325 + 500×5.6²	Completion of module (0) motion through pipeline 9 (3.7 m) to nozzle (0.6607 s, speed 5.6 m/s, pressure 19.1 atm). End of startup cycle (0).
2.9537027	78.48	15.1	7 966 601	(78.48-1)×101325 + 500×15.1²	Completion of module (1) motion through pipeline 9 (3.7 m) to nozzle (0.245033 s, speed 15.1 m/s, pressure 78.48 atm) after stabilization. End of nominal cycle (1).
3.1223444	1.0	–	0	(1-1)×101325 + 500×0²	Module (2) moved into pipeline 9 through valve 7 (0.17341 s), module speed 15.1 m/s, pressure 96.4 atm, module tail).
3.1247644	1.0	–	0	(1-1)×101325 + 500×0²	Closing of valve 7 disc. Closing time 0.00242 s. Vacuum phase in pipeline 3 (-0.8 atm). Flow in pipeline (1) stopped. Opening of valve 2 (0.008896 s). Start of nominal cycle (3).
3.1336604	1.0	–	0	(1-1)×101325 + 500×0²	Valve 2 disc opened. Resumption of continuous flow in pipelines 1 and 3. Continuous flow 13.42 m/s restored. Travel time to valve 4 (0.223547 s).
3.3572074	1.0	–	0	(1-1)×101325 + 500×0²	Continuous flow near valve 4 disc. Disc closing. Closing time 0.00134 s.
3.3585474	1.0	–	0	(1-1)×101325 + 500×0²	Hydraulic shock at valve 4. Pressure amplitude 120.5 atm. First flow interruption. Flow deceleration and stop. Formation of small module (3) in drain pipeline 5: Nominal cycle: volume = 0.26 L, ejection speed = 32.8 m/s. Module is discharged to atmosphere through spring damper 15, Laval nozzle 16 and hydraulic seal 6 (L5 = 4.7 m). Opening of valve 7 disc.

Time, s	p(t), atm	v(t), m/s	ε(t), J/m³	Calculation ε(t), (J/m³) ε(t) = ΔP(t) + ρ·v(t)²/2 = (P(t)-1)×101325 + 500·v(t)²	Note
3.3601957	1.0	–	0	(1-1)×101325 + 500×0²	Shock wave front (0.0016483 s) at control point A3.
3.3618441	1.0	–	0	(1-1)×101325 + 500×0²	Shock wave front from valve 4 disc reaches valve 2 disc (0.0032967 s).
3.3626091	1.0	–	0	(1-1)×101325 + 500×0²	Hydraulic shock at valve 2. Disc closing time 0.000765 s. Pressure amplitude 120 atm. Second flow interruption. Formation of module (3) 141.3 L in pipeline 3. Start of module (3) motion in pipeline 3 (L3=3 m; v=17.3 m/s).
3.3633351	1.0	–	0	(1-1)×101325 + 500×0²	Shock wave front (0.000726 s) from valve 2 disc reaches control point A1. Passage of shock wave front to spring hydraulic pulse pressure amplitude damper (17) in supply pipeline (1) and to the second bottom of reservoir R1. Flow deceleration of 222.1 L in pipeline 1.
3.3648069	1.0	–	0	(1-1)×101325 + 500×0²	Shock wave front (0.0021978 s) from valve 2 disc reaches the second bottom of reservoir R1, damped to pressure 1.887 atm. Flow in pipeline (1) stopped. Valve 2 closed.
3.3673774	78.48	15.1	7 966 601	(78.48-1)×101325 + 500×15.1²	Completion of module (2) motion through pipeline 9 (3.7 m) to nozzle (0.245033 s, speed 15.1 m/s, pressure 78.48 atm) after pressure stabilization. End of nominal cycle (2).
3.5360191	1.0	–	0	(1-1)×101325 + 500×0²	Module (3) moved into pipeline 9 through valve 7 (0.17341 s), module speed 15.1 m/s, pressure 96.4 atm. Module tail).

Table A.5.4 – Point **A5** (control/drain branch outlet).

Time, s	p(t), atm	v(t), m/s	ε(t), J/m³	Calculation ε(t), (J/m³) ε(t) = ΔP(t) + ρ·v(t)²/2 = (P(t)-1)×101325 + 500·v(t)²	Note
0	1.0	–	0	(1-1)×101325 + 500×0²	Start of continuous flow of 222.1 L from reservoir R1 through pipeline 1.
0.3906	1.0	–	0	(1-1)×101325 + 500×0²	no water. Continuous flow 222.1 L at point A1 of pipeline 1.
0.639	1.0	–	0	(1-1)×101325 + 500×0²	no water. Continuous flow 222.1 L at point B (valve 2) of pipeline 3.
1.203	1.0	–	0	(1-1)×101325 + 500×0²	no water. Continuous flow 222.1 L at control point A3 of pipeline 3 before valve 4.
1.766917	1.0	–	0	(1-1)×101325 + 500×0²	no water. Continuous flow 222.1 L before hydraulic shock at valve 4. Disc closing time (0.00303 s).
1.769947	1.0	–	0	(1-1)×101325 + 500×0²	Hydraulic shock at valve 4. Pressure amplitude 23.9 atm. First flow interruption. Formation of small module (0) in drain pipeline 5: Startup cycle: volume = 0.12 L, ejection speed = 11.2 m/s. Module is discharged to atmosphere through spring damper 15, Laval nozzle 16 and hydraulic seal 6 (L5 = 4.7 m). Flow deceleration and stop. Opening of valve 7 disc.
1.771596	1.0	–	0	(1-1)×101325 + 500×0²	Shock wave front (0.0016483 s) at control point A3.
1.7732437	23.9	–	2 320342.5	(23.9-1)×101325 + 500×0²	Shock wave front from valve 4 disc reaches valve 2 disc (0.0032967 s). Shock wave front (0.0032967 s) at control point A5.
1.7749537	1.0	–	0	(1-1)×101325 + 500×0²	Hydraulic shock at valve 2. Disc closing time 0.00171 s. Second flow interruption. Formation of module (0) 141.3 L in pipeline 3. Start of module (0) motion in pipeline 3 (L3=3 m; v=5.8 m/s).
1.7756797	1.0	–	0	(1-1)×101325 + 500×0²	Shock wave front (0.000726 s) from valve 2 disc reaches control point A1. Passage of shock wave front to spring hydraulic pulse pressure amplitude damper (17) in supply pipeline (1) and to the second bottom of reservoir R1. Flow deceleration of 222.1 L in pipeline 1.
1.7771515	1.0	–	0	(1-1)×101325 + 500×0²	Shock wave front (0.0021978 s) from valve 2 disc reaches the second bottom of reservoir R1, damped to pressure 1.887 atm. Flow in pipeline (1) stopped. Valve 2 closed.
2.03775	19.6	10.1	1 935 650	(19.6-1)×101325 + 500×10.1²	Small module (0) at control point A5.
2.20607	1.0	–	–	(1-1)×101325 + 500×0²	Completion of small module (0). Discharge to atmosphere (or lower reservoir) of small module (0) with pressure reduction in pipeline 5 to ~1 atm and flow speed reduced to natural gravitational value; hydraulic seal 6 prevents air intake.
2.2921947	1.0	–	0	(1-1)×101325 + 500×0²	Module (0) moved into pipeline 9 through valve 7 (0.517241 s), module speed 5.6 m/s, 19.1 atm, module tail).
2.2974147	1.0	–	0	(1-1)×101325 + 500×0²	Closing of valve 7 disc. Closing time 0.00522 s. Vacuum phase in pipeline 3 (-0.8 atm). Flow in pipeline (1) stopped. Opening of valve 2 (0.008896 s). Start of nominal cycle (1).
2.3063107	1.0	–	0	(1-1)×101325 + 500×0²	Valve 2 disc opened. Resumption of continuous flow in pipelines 1 and 3. Continuous flow 13.42 m/s. Travel time to valve 4: 0.223547 s.
2.529858	1.0	–	0	(1-1)×101325 + 500×0²	Continuous flow near valve 4 disc. Disc closing (0.00134 s).
2.531198	1.0	–	0	(1-1)×101325 + 500×0²	Hydraulic shock at valve 4. Pressure amplitude 120.5 atm. First flow interruption. Flow deceleration and stop. Formation of small module (1) in drain pipeline 5: Nominal cycle: volume = 0.26 L, ejection speed = 32.8 m/s. Module is discharged to atmosphere through spring damper 15, Laval nozzle 16 and hydraulic seal 6 (L5 = 4.7 m). Opening of valve 7 disc.

2.5328463	1.0	–	0	(1-1)×101325 + 500×0²	Shock wave front (0.0016483 s) at control point A3.
2.5344947	120.5	–	12 108 337	(120.5-1)×101325 + 500×0²	Shock wave front from valve 4 disc reaches valve 2 disc (0.0032967 s). Shock wave front (0.0032967 s) at control point A5.
2.5352597	1.0	–	0	(1-1)×101325 + 500×0²	Hydraulic shock at valve 2. Disc closing time 0.000765 s. Pressure amplitude 120 atm. Second flow interruption. Formation of module (1) 141.3 L in pipeline (3). Start of module (1) motion in pipeline (3): (L3=3 m; v=17.3 m/s).
2.5359857	1.0	–	0	(1-1)×101325 + 500×0²	Shock wave front from valve 2 disc (0.661 m) reaches control point A1 (0.000726 s). Passage of shock wave front to spring hydraulic pulse pressure amplitude damper (17) in supply pipeline (1) and to the second bottom of reservoir R1. Flow deceleration of 222.1 L in pipeline 1.
2.5374575	1.0	–	0	(1-1)×101325 + 500×0²	Shock wave front (0.0021978 s) from valve 2 disc reaches the second bottom of reservoir R1, damped to pressure 1.887 atm. Flow in pipeline (1) stopped. Valve 2 closed.
2.622598	96.4	28.1	10 061 210	(96.4-1)×101325 + 500×28.1²	Small module (1) at control point A5.
2.68309	1.0	–	0	(1-1)×101325 + 500×0²	Completion of small module (1). Discharge to atmosphere (or lower reservoir) of small module (1) with pressure reduction in pipeline 5 to ~1 atm and flow speed reduced to natural gravitational value; hydraulic seal 6 prevents air intake.
2.7086697	1.0	–	0	(1-1)×101325 + 500×0²	Module (1) moved into pipeline 9 through valve 7 (0.17341 s), module speed 15.1 m/s, pressure 96.4 atm, module tail).
2.7110897	1.0	–	0	(1-1)×101325 + 500×0²	Closing of valve 7 disc. Closing time 0.00242 s. Vacuum phase in pipeline 3 (-0.8 atm). Flow in pipeline (1) stopped. Opening of valve 2 (0.008896 s). Start of nominal cycle (2).
2.7199857	1.0	–	0	(1-1)×101325 + 500×0²	Valve 2 disc opened. Resumption of continuous flow in pipelines 1 and 3. Continuous flow 13.42 m/s restored. Travel to valve 4 (0.223547 s).
2.9435327	1.0	–	0	(1-1)×101325 + 500×0²	Continuous flow near valve 4 disc. Disc closing, closing time 0.00134 s.
2.9448727	1.0	–	0	(1-1)×101325 + 500×0²	Hydraulic shock at valve 4. Pressure amplitude 120.5 atm. First flow interruption. Flow deceleration and stop. Formation of small module (2) in drain pipeline 5: Nominal cycle: volume = 0.26 L, ejection speed = 32.8 m/s. Module is discharged to atmosphere through spring damper 15, Laval nozzle 16 and hydraulic seal 6 (L5 = 4.7 m). Opening of valve 7 disc.
2.9465210	1.0	–	0	(1-1)×101325 + 500×0²	Shock wave front (0.0016483 s) at control point A3 (1.5 m).
2.9481694	120.5	–	12 108 337	(120.5-1)×101325 + 500×0²	Shock wave front from valve 4 disc reaches valve 2 disc (0.0032967 s), 3 m. Shock wave front (0.0032967 s) at control point A5.
2.9489344	1.0	–	0	(1-1)×101325 + 500×0²	Hydraulic shock at valve 2. Disc closing time 0.000765 s. Pressure amplitude 120 atm. Second flow interruption. Formation of module (2) 141.3 L in pipeline 3. Start of module (2) motion in pipeline 3 (L3=3 m; v=17.3 m/s).
2.9496604	1.0	–	0	(1-1)×101325 + 500×0²	Shock wave front (0.000726 s) from valve 2 disc reaches control point A1. Passage of shock wave front to spring hydraulic pulse pressure amplitude damper (17) in supply pipeline (1) and to the second bottom of reservoir R1. Flow deceleration of 222.1 L in pipeline 1.
2.9511322	1.0	–	0	(1-1)×101325 + 500×0²	Shock wave front (0.0021978 s) from valve 2 disc reaches the second bottom of reservoir R1, damped to pressure 1.887 atm. Flow in pipeline (1) stopped. Valve 2 closed.
2.9528947	1.0	–	0	(1-1)×101325 + 500×0²	Completion of module (0) motion through pipeline 9 (3.7 m) to nozzle (0.6607 s, speed 5.6 m/s, pressure 19.1 atm). End of startup cycle (0).
2.9537027	1.0	–	0	(1-1)×101325 + 500×0²	Completion of module (1) motion through pipeline 9 (3.7 m) to nozzle (0.245033 s, speed 15.1 m/s, pressure 78.48 atm) after stabilization. End of nominal cycle (1).
3.0362727	96.4	28.1	10 061 210	(96.4-1)×101325 + 500×28.1²	Small module (2) at control point A5.
3.0967647	1.0	–	0	(1-1)×101325 + 500×0²	Completion of small module (2). Discharge to atmosphere (or lower reservoir) of small module (2) with pressure reduction in pipeline 5 to ~1 atm and flow speed reduced to natural gravitational value; hydraulic seal 6 prevents air intake.
3.1223444	1.0	–	0	(1-1)×101325 + 500×0²	Module (2) moved into pipeline 9 through valve 7 (0.17341 s), module speed 15.1 m/s, pressure 96.4 atm, module tail).
3.1247644	1.0	–	0	(1-1)×101325 + 500×0²	Closing of valve 7 disc. Closing time 0.00242 s. Vacuum phase in pipeline 3 (-0.8 atm). Flow in pipeline (1) stopped. Opening of valve 2 (0.008896 s). Start of nominal cycle (3).
3.1336604	1.0	–	0	(1-1)×101325 + 500×0²	Valve 2 disc opened. Resumption of continuous flow in pipelines 1 and 3. Continuous flow 13.42 m/s restored. Travel time to valve 4 (0.223547 s).
3.3572074	1.0	–	0	(1-1)×101325 + 500×0²	Continuous flow near valve 4 disc. Disc closing. Closing time 0.00134 s.
3.3585474	1.0	–	0	(1-1)×101325 + 500×0²	Hydraulic shock at valve 4. Pressure amplitude 120.5 atm. First flow interruption. Flow deceleration and stop. Formation of small module (3) in drain pipeline 5: Nominal cycle: volume = 0.26 L, ejection speed = 32.8 m/s. Module is discharged to atmosphere through spring damper 15, Laval nozzle 16 and hydraulic seal 6 (L5 = 4.7 m). Opening of valve 7 disc.
3.3601957	1.0	–	0	(1-1)×101325 + 500×0²	Shock wave front (0.0016483 s) at control point A3.
3.3618441	120.5	–	12 108 337	(120.5-1)×101325 + 500×0²	Shock wave front from valve 4 disc reaches valve 2 disc (0.0032967 s). Shock wave front (0.0032967 s) at control point A5.
3.3626091	1.0	–	0	(1-1)×101325 + 500×0²	Hydraulic shock at valve 2. Disc closing time 0.000765 s. Pressure amplitude 120 atm. Second flow interruption. Formation of module (3)

					141.3 L in pipeline 3. Start of module (3) motion in pipeline 3 (L3=3 m; v=17.3 m/s).
3.3633351	1.0	–	0	(1-1)×101325 + 500×0²	Shock wave front (0.000726 s) from valve 2 disc reaches control point A1. Passage of shock wave front to spring hydraulic pulse pressure amplitude damper (17) in supply pipeline (1) and to the second bottom of reservoir R1. Flow deceleration of 222.1 L in pipeline 1.
3.3648069	1.0	–	0	(1-1)×101325 + 500×0²	Shock wave front (0.0021978 s) from valve 2 disc reaches the second bottom of reservoir R1, damped to pressure 1.887 atm. Flow in pipeline (1) stopped. Valve 2 closed.
3.3673774	1.0	–	0	(1-1)×101325 + 500×0²	Completion of module (2) motion through pipeline 9 (3.7 m) to nozzle (0.245033 s, speed 15.1 m/s, pressure 78.48 atm) after pressure stabilization. End of nominal cycle (2).
3.4499474	96.4	28.1	10 061 210	(96.4-1)×101325 + 500×28.1²	Small module (3) at control point A5.
3.5104394	1.0	–	0	(1-1)×101325 + 500×0²	Completion of small module (3). Discharge to atmosphere (or lower reservoir) of small module (3) with pressure reduction in pipeline 5 to ∼1 atm and flow speed reduced to natural gravitational value; hydraulic seal 6 prevents air intake.
3.5360191	1.0	–	0	(1-1)×101325 + 500×0²	Module (3) moved into pipeline 9 through valve 7 (0.17341 s), module speed 15.1 m/s, pressure 96.4 atm. Module tail.

ACKNOWLEDGMENTS

The author thanks the hydraulic engineering community for valuable discussions on transient flow phenomena and energy conservation principles.

CONFLICT OF INTEREST STATEMENT

The patent for the GIF² system [26] was filed by Orlov and is licensed to FLOW JET ENERGY LTD, where the author serves as Managing Director. The author declares that the research was conducted with full scientific objectivity and transparency.

DATA AVAILABILITY STATEMENT

The numerical data supporting the findings of this study (complete time-series datasets for p(t), v(t), and ε(t) at all control points) are available from the corresponding author upon reasonable request.

END OF MANUSCRIPT v5.2– 12.02.2026

Author: Valerii Orlov
Managing Director, FLOW JET ENERGY LTD
Tel.: (+380) 95 338 91 22
E-mail: rst.hspp@gmail.com